NUMERICAL EVALUATION OF THE VALIDITY DOMAIN OF LORENZ EQUATIONS

By:

Allison Lindgren

A Thesis

Submitted in Partial Fulfillment

of the Requirements for the Degree of

Master of Science in

Mechanical Engineering

Northern Arizona University

May 2018

Approved:

Dr. Peter Vadasz, Chair

Dr. James Swift, Committee member

Dr. Tom Acker, Committee member

ABSTRACT

Natural convection in a two-dimensional rectangular domain heated at the bottom and cooled at the top with perfectly insulated sidewalls is the topic of interest for this research. For Rayleigh numbers less than the critical value, Ra_{cr}, any disturbances will decay to a motionless solution and heat transfer will occur via conduction only. Above Ra_{cr}, natural convection develops in the domain. At some second critical Rayleigh number, Ra_t, the steady convection cells lose stability and the solution transitions to a weakly turbulent (chaotic) state. The Lorenz system was previously derived from the governing equations using a truncated Galerkin expansion. This research investigates the validity domain of the Lorenz system as a model for natural convection in porous media. The temperature and velocity fields given by the Lorenz system are compared to a numerical solution for the temperature and velocity fields for increasing Rayleigh numbers. Results show that near $Ra = 80$ the number of convection cells predicted by the numerical solution increases from two to three as a result of the chosen wavenumber becoming unstable. The result is a significant difference between the Lorenz system and the numerical solution. To provide a comparison between the Lorenz solution and the numerical solution that is global in scale relative to the problem domain, we compared the Nusselt numbers resulting from each solution to experimental data.

TABLE OF CONTENTS

LIST OF FIGURES

LIST OF TABLES

NOMENCLATURE

Φ	Porosity	x	
k	Permeability	y	Length dimensions
γ_f	Heat capacity of saturating fluid	z	
γ_e	Effective heat capacity	$\boldsymbol{V}$	Filtration velocity vector
M_f	Defined as $\frac{\gamma_f}{\gamma_e}$	u	Filtration velocity in x-direction
ρ_s	Density of solid structure	v	Filtration velocity in y-direction
ρ_f	Density of saturating fluid	w	Filtration velocity in z-direction
$C_{p,s}$	Specific heat of solid structure	t	Time
$C_{p,f}$	Specific heat of saturating fluid	$\hat{e}_x$	Unit vector in x-direction
K_s	Thermal conductivity of solid structure	$\hat{e}_y$	Unit vector in y-direction
K_f	Thermal conductivity of saturating fluid	$\hat{e}_z$	Unit vector in z-direction
K_e	Effective thermal conductivity	$\hat{e}_g$	Unit vector in direction of gravity
α_e	Effective thermal diffusivity	g	Magnitude of gravity
β	Thermal expansion coefficient of saturating fluid	H	Height of problem domain
p_r	Reduced pressure	L	Length of problem domain
ν	Kinematic viscosity of saturating fluid	h^*	Height of convection cell
$\bar{h}$	Conductive heat transfer coefficient	l^*	Length of convection cell
Ra	Rayleigh number	V	Volume
Ra_{cr}	Critical Rayleigh number	D	Diameter
Va	Vadasz number	T	Temperature
Da	Darcy number	Ψ	Stream function
Pr_D	Darcy-Prandtl number	M	Number of computational nodes in x-direction

A_{11}	Coefficients of Galerkin expansion	N	Number of computational nodes in z-direction
B_{11}		T_{MS}	Manufactured solution for temperature
B_{02}		Ψ_{MS}	Manufactured solution for stream function
X		Q_T	Source term for temperature
Y	Coefficients of Galerkin expansion, scaled relative to fixed points	Q_Ψ	Source term for stream function
Z		h	Grid refinement parameter, defined as $h = \sqrt{L/N}$
R	Scaled Rayleigh number	π	Ratio of a circle's circumference to its diameter
α	Scaled Vadasz number	e	Euler's constant
κ	Lorenz system wavenumber		

1 INTRODUCTION

Porous media is used extensively to control heat flow, with porous media heat exchangers and clothing being notable examples [1]. Analysis of convection in porous media is also essential when predicting the output of geothermal systems [2]. Since porous media is often used to control heat and energy transfer, understanding the underlying processes governing heat transfer in porous media is of significant engineering interest.

It is well known that fluid flow in porous media for low Reynolds numbers is governed by Darcy's Law – a volumetric averaged version of Navier-Stokes. This was first established experimentally by Darcy [3] and the conservation equations for porous media are known as Darcy's Law. Although Darcy's Law was first established in 1856, the relationship between conductive and convective heat transfer in porous media is still an ongoing topic of research.

Vadasz and Olek [4] used a Galerkin expansion to derive an analytical solution to the equations governing natural convection in porous media. In their research, Vadasz and Olek [4] showed that this solution was equivalent to the Lorenz equations, which were first derived as a simplified model of atmospheric convection [5]. The purpose of the present research is to determine the range of Rayleigh numbers for which this solution is valid. This is done in the following ways:

1. The general governing equations from which the Lorenz equations were derived are solved using a finite difference scheme. The results for the stream function and temperature from the Lorenz equations are directly compared to the results from the numerical solution for $40 \leq Ra \leq 100$.
2. The Nusselt number (dimensionless heat flux) is calculated, using the results from both solutions. These results are compared to existing experimental data.

Background

To provide the reader with sufficient background information, the key assumptions used when deriving the governing equations, which are specific to natural convection in porous media are outlined in this section. Sufficient information is provided so that a reader with a background in fluid mechanics and heat transfer can extend the necessary principles to porous media.

A material with solid phase and a fluid phase where both phases are interconnected is considered a porous media. Examples of porous media range from soil and gravel to clothing and hair. The individual pores can take on virtually any combination of shapes and sizes, from highly structured configurations with uniform pores to unstructured configurations with a range of pore sizes. A specific porous media is described in terms of its porosity and permeability. Porosity, Φ is defined as the ratio of the total pore volume to the total overall volume of the porous structure. It is a non-dimensional value which describes the overall relative volume of the pores.

$$\Phi = \frac{V_{pores}}{V_{total}} \tag{1.1}$$

Permeability, k describes how well a fluid is able to move through a porous domain and has units of [m^2]. The permeability of a porous structure depends not only on how large the pores are but also on the shape and configuration of those pores. If k varies over the domain, i.e. $k = k(x, y, z)$ the porous structure is heterogeneous. If k is constant over the domain the porous structure is homogeneous. For this research, it is assumed that the porous structure is homogeneous.

Thermal properties

The thermal characteristics of a porous structure saturated with fluid are described as a combination of the thermal properties of the solid material which forms the structure and the thermal properties of the saturating fluid. The saturated porous structure consists of both a solid and fluid part, and the effective heat capacity of the overall structure, γ_e is defined as follows:

$$\gamma_e = (1 - \Phi)\rho_s C_{P,s} + \Phi\rho_f C_{p,f} \tag{1.2}$$

The $(1 - \Phi)$ term represents the fraction of the volume consisting of the solid structure, and Φ represents the fraction of the volume consisting of the saturating fluid. Similarly, the effective thermal conductivity and the effective thermal diffusivity, K_e and α_e respectively, are defined as

$$K_e = (1 - \Phi)K_s + \Phi K_f \tag{1.3}$$

$$\alpha_e = \frac{K_e}{\gamma_e} \tag{1.4}$$

Describing heat transfer in porous media is somewhat more complex when the saturating fluid is moving, as the temperature of the solid structure and the saturating fluid must be tracked, as well as the heat transfer that occurs between the two. If the fluid motion is sufficiently slow, and the average pore size of the porous medium is sufficiently small, it can be assumed that the average local temperature of the solid porous structure is equal to the local average temperature of the saturating fluid for a representative elementary volume (REV). This approximation is called "local thermal equilibrium" and is one assumption used for this research. This allows the analysis to be substantially simplified, and then the energy balance equation emerges

$$\frac{\partial T}{\partial t} + M_f \boldsymbol{V} \cdot \nabla T = \alpha_e \nabla^2 T \tag{1.5}$$

This research specifically explores the characteristics of natural convection in porous media. Natural convection occurs when density variations in a fluid subject to gravity, usually caused by uneven heating or cooling, cause fluid motion. Forced convection occurs when the fluid motion is the result of some outside force and is not considered here.

Non-Dimensional Parameters

Natural convective flow is driven by the buoyancy forces that develop when a fluid is heated from below. The Rayleigh number represents the ratio of buoyancy forces to viscous forces and is the most important non-dimensional parameter for determining the nature of natural convective flow. For natural convective flow in porous media the Rayleigh number is modified to include porosity.

$$Ra = \frac{\beta \Delta T g H \kappa M_f}{\alpha_e \nu} \tag{1.6}$$

The Rayleigh number determines whether buoyancy forces or viscous forces will dominate the fluid flow. Below the critical Rayleigh number, Ra_{cr}, no convection will occur. The critical Rayleigh number for natural convection in porous media is $Ra_{cr} = 4 \cdot \pi^2$. Weak non-linear analysis of the equations governing natural convection in porous media show that when the Rayleigh number reaches the critical value, a pitchfork bifurcation occurs. At this point, depending on the initial conditions, natural convection occurs with either clockwise or counterclockwise rotation of convection cells. Chapter 4 describes this phenomenon in detail.

Convection motion results in an overall increase in average heat transfer. The Nusselt number is a non-dimensional number which represents the ratio of convective heat transfer to conductive heat transfer.

$$Nu = \frac{\bar{h} \cdot L}{K_e} \tag{1.7}$$

As convection in a fluid becomes more dominant, the Nusselt number increases. A system characterized by a sudden onset of natural convection will have a Nusselt number of one up to the point when natural convection occurs, at which point the Nusselt number rises steadily with the Rayleigh number. After the onset of convection, it has been shown analytically and experimentally that the Nusselt number is a function of the Rayleigh number [2], [6]–[8].

It was shown [4], [9], [10] that when investigating wave phenomena, the time derivative term which is typically ignored in Darcy's equation cannot be neglected. This term is expressed in dimensionless form as $\frac{\Phi \mathrm{Pr_D}}{Da}$ and is now known as the Vadasz number.

$$Va = \frac{\Phi Pr_D}{Da} = \frac{\Phi H^2 \nu}{\alpha_e \kappa} \tag{1.8}$$

Convective cell patterns

Chandrasekhar [11] described two distinct behaviors often arise when studying natural convection in a pure fluid: Longitudinal rolls, shown in Figure 1.1, and polyhedral convective cells, shown in Figure 1.2. Longitudinal rolls are 2D convective cells. The aspect ratio of these type of cells is ${l^*}/{h^*} = 1$. Polyhedral convective cells may also form when the Rayleigh number

is close to the critical Rayleigh number. This type of convection cell has an aspect ratio of $l^*/h^* = 1.33$. As the Rayleigh number increases, the length of the convection cells will decrease slightly. Combarnous and Borries [8] showed that the same principles apply for natural convection in porous media.

LONGITUDINAL CONVECTION CELLS

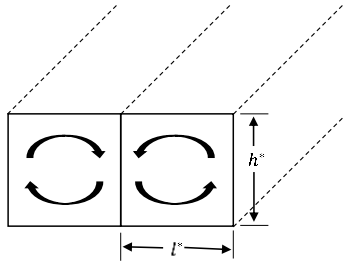

Figure 1.1: Longitudinal convective cells.

POLYHEDRAL CONVECTION CELLS

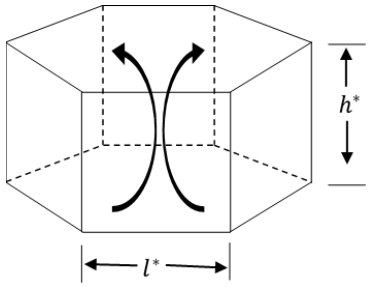

Figure 1.2: Polyhedral convective cells.

Strauss [12] showed that 2D convection is stable for Rayleigh numbers $Ra_{cr} < Ra < 9 \cdot Ra_{cr}$. Thus, for the purposes of this research, it is assumed that 2D longitudinal rolls occur.

2 PROBLEM FORMULATION

Overview

A porous layer saturated with a stationary fluid is heated from below and cooled from above, as presented in Figure 2.1. The layer is subject to gravity, which is in the z-direction only, i.e. $\hat{\boldsymbol{e}}_g = -\hat{\boldsymbol{e}}_z$, where $\hat{\boldsymbol{e}}_g$ is a unit vector in the direction of the acceleration of gravity and $\hat{e}_z$ is the unit vector in the z-direction. It is assumed that Darcy's law governs the flow except that the time derivative term is not neglected. This was shown to be necessary by Vadasz and Olek [4], [9], [10] when studying wave phenomena and is known as the extended Darcy equation. The fluid is assumed to be incompressible, and the Boussinesq approximation is applied to account for the effects of density variations, which means that the density is assumed to be constant everywhere except in the gravity term in the extended Darcy equation.

Governing Equations

The system described above is governed by the following set of non-dimensional equations:

Continuity Equation

$$\nabla \cdot \boldsymbol{V} = 0 \tag{2.1}$$

Conservation of Momentum (Extended Darcy's Law)

$$\frac{1}{Va}\frac{\partial \boldsymbol{V}}{\partial t} + \boldsymbol{V} = -\nabla p_r + Ra T \hat{\boldsymbol{e}}_z \tag{2.2}$$

Conservation of Energy

$$\frac{\partial T}{\partial t} + \boldsymbol{V} \cdot \nabla T = \nabla^2 T \tag{2.3}$$

Where $\boldsymbol{V} = u\hat{\boldsymbol{e}}_x + v\hat{\boldsymbol{e}}_y + w\hat{\boldsymbol{e}}_z$ and $\hat{\boldsymbol{e}}_x$, $\hat{\boldsymbol{e}}_y$, $\hat{\boldsymbol{e}}_z$ are unit vectors in the x, y, and z directions, respectively, and p_r is the reduced pressure. The non-dimensional terms are defined as follows:

Darcy Number

$$Da = \frac{k}{L^2} \tag{2.4}$$

Prandtl Number

$$Pr_D = \frac{\nu}{\alpha_e} \tag{2.5}$$

Vadasz Number

$$Va = \frac{\Phi Pr_D}{Da} \tag{2.6}$$

Rayleigh Number

$$Ra = \frac{\beta \Delta T_c k H M_f}{\nu \alpha_e} \tag{2.7}$$

PROBLEM DOMAIN

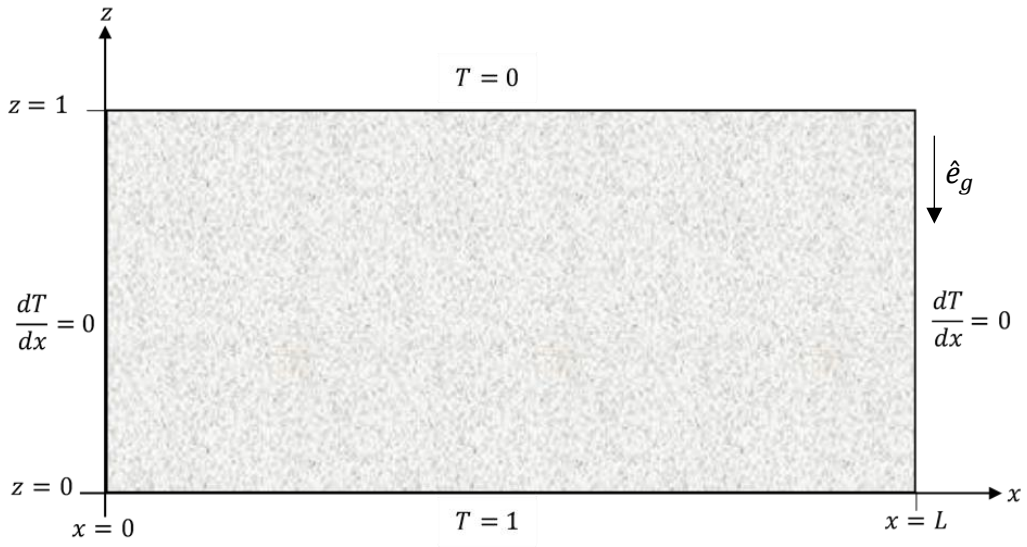

Figure 2.1: The problem domain for which the governing equations are solved, with boundary conditions.

It is assumed that the flow pattern will be 2-dimensional longitudinal rolls. Consequently, a 2D flow simplification is applied and the stream function is introduced, which can be applied to any 2D incompressible flow.

Assumptions

No flow in y-direction

$$v = 0 \tag{2.8}$$

$$\frac{\partial(\cdot)}{\partial y} = \frac{\partial^2(\cdot)}{\partial y^2} = 0 \tag{2.9}$$

Definition of Stream Function

$$u = \frac{\partial \Psi}{\partial z} \tag{2.10}$$

$$w = -\frac{\partial \Psi}{\partial x} \tag{2.11}$$

The stream function identically satisfies the continuity equation.

Initial and boundary conditions

As shown in Figure 2.1, the problem domain is a rectangular porous domain with dimensionless height $H = 1$ and dimensionless length L (aspect ratio). The top and bottom are kept at constant temperatures, $T = 0$ and $T = 1$, respectively. The side walls are insulated, so that there is zero heat flux through the side walls. The impermeability condition is applied at the walls, so that the filtration velocity perpendicular to the walls is zero, i.e. $u = 0$ at the vertical walls and $w = 0$ at the horizontal walls.

$x = 0$:

$$u = 0 \Rightarrow \Psi = 0 \tag{2.12}$$

$$\frac{dT}{dx} = 0 \tag{2.13}$$

$x = L$:

$$u = 0 \Rightarrow \Psi = 0 \tag{2.14}$$

$$\frac{dT}{dx} = 0 \tag{2.15}$$

$z = 0$:

$$w = 0 \Rightarrow \Psi = 0 \tag{2.16}$$

$$T = 1 \tag{2.17}$$

$z = 1$:

$$w = 0 \Rightarrow \Psi = 0 \tag{2.18}$$

$$T = 0 \tag{2.19}$$

The fluid inside the porous domain is initially stationary at all points with a temperature of $T = 0$ at all points except at $z = 0$.

$t = 0$:

$$z = 0: \qquad T = 1 \tag{2.20}$$

$$0 \leq z \leq 1: \qquad u = w = 0 \Rightarrow \Psi = 0 \tag{2.21}$$

Simplification of governing equations

Conservation of Mass

The 2D flow assumption and stream function simplification are applied to the continuity equation by substituting equations (2.10) and (2.11) into (2.1),

$$\frac{\partial^2 \Psi}{\partial x \partial z} - \frac{\partial^2 \Psi}{\partial x \partial z} = 0 \tag{2.22}$$

Equation (2.22) shows that the equation representing conservation of mass is identically satisfied by the definition of the stream function. This reduces the number of equations that need to be solved.

Extended Darcy's Law

Equation (2.2) is in vector form and can be broken into x, y, and z components,

x-direction
$$\frac{1}{Va}\frac{\partial u}{\partial t} + u = -\frac{\partial p_r}{\partial x} \tag{2.23}$$

y-direction
$$\frac{1}{Va}\frac{\partial v}{\partial t} + v = -\frac{\partial p_r}{\partial x} \tag{2.24}$$

z-direction
$$\frac{1}{Va}\frac{\partial w}{\partial t} + w = -\frac{\partial p_r}{\partial z} + Ra \cdot T \tag{2.25}$$

The 2D flow assumption and introduction of the stream function are applied to the extended Darcy's Law by substituting equations (2.8) through (2.11) into equations (2.23), (2.24), and (2.25),

x-direction
$$\frac{1}{Va}\frac{\partial^2 \Psi}{\partial t \partial z} + \frac{\partial \Psi}{\partial z} = -\frac{\partial p_r}{\partial x} \tag{2.26}$$

y-direction
$$0 = 0 \tag{2.27}$$

z-direction
$$-\frac{1}{Va}\frac{\partial^2 \Psi}{\partial t \partial x} - \frac{\partial \Psi}{\partial x} = -\frac{\partial p_r}{\partial z} + Ra \cdot T \tag{2.28}$$

It is advantageous to combine equations (2.28) and (2.26), which can be done as follows,

$$\frac{\partial}{\partial z}(2.26) \Rightarrow \frac{1}{Va}\frac{\partial^3 \Psi}{\partial t \partial z} + \frac{\partial^2 \Psi}{\partial z^2} = -\frac{\partial^2 p_r}{\partial x \partial z} \tag{2.29}$$

$$\frac{\partial}{\partial x}(2.28) \Rightarrow \frac{1}{Va}\frac{\partial^3 \Psi}{\partial t \partial x^2} + \frac{\partial^2 \Psi}{\partial x^2} = -\frac{\partial^2 p_r}{\partial z \partial x} + Ra \cdot T \tag{2.30}$$

$$(2.29) - (2.30) \Rightarrow \frac{1}{Va}\frac{\partial}{\partial t}\left(\frac{\partial^2 \Psi}{\partial x^2} + \frac{\partial^2 \Psi}{\partial z^2}\right) + \left(\frac{\partial^2 \Psi}{\partial x^2} + \frac{\partial^2 \Psi}{\partial z^2}\right) = -Ra\frac{dT}{dx} \tag{2.31}$$

Equation (2.31) is the final simplified form for the extended Darcy's Law.

Conservation of Energy

The 2D flow assumption and the introduction of the stream function are applied to the continuity equation by substituting equations (2.8) through (2.11) into (2.3),

$$\frac{\partial T}{\partial t} + \frac{\partial \Psi}{\partial z}\frac{\partial T}{\partial x} - \frac{\partial \Psi}{\partial x}\frac{\partial T}{\partial z} = \frac{\partial^2 T}{\partial x^2} + \frac{\partial^2 T}{\partial z^2} \tag{2.32}$$

Equation (2.32) is the final simplified form of conservation of energy.

Summary

The resulting system consists of two equations with two unknown variables, temperature (T) and the stream function (Ψ). The equations vary in two spatial dimensions, x and z, and are time dependent. The two equations are also coupled, which means that one equation cannot be solved without the solution to the other for any point in space and time.

Governing Equations

$$\frac{1}{Va}\frac{\partial}{\partial t}\left(\frac{\partial^2\Psi}{\partial x^2}+\frac{\partial^2\Psi}{\partial z^2}\right)+\left(\frac{\partial^2\Psi}{\partial x^2}+\frac{\partial^2\Psi}{\partial z^2}\right)=-Ra\frac{dT}{dx} \tag{2.33}$$

$$\frac{\partial T}{\partial t}+\frac{\partial\Psi}{\partial z}\frac{\partial T}{\partial x}-\frac{\partial\Psi}{\partial x}\frac{\partial T}{\partial z}=\frac{\partial^2 T}{\partial x^2}+\frac{\partial^2 T}{\partial z^2} \tag{2.34}$$

Initial Conditions

$t = 0$:

$$T = 0 \tag{2.35}$$

Boundary Conditions

$x = 0$:

$$\Psi = 0 \tag{2.36}$$

$$\frac{dT}{dx} = 0 \tag{2.37}$$

$x = L$:

$$\Psi = 0 \tag{2.38}$$

$$\frac{dT}{dx} = 0 \tag{2.39}$$

$z = 0$:

$$\Psi = 0 \tag{2.40}$$

$$T = 1 \tag{2.41}$$

$z = 1$:

$$\Psi = 0 \tag{2.42}$$

$$T = 0 \tag{2.43}$$

3 LITERATURE REVIEW

Much work has been done to obtain an analytical solution for natural convection in porous media. When the assumption is made that 2D longitudinal convective rolls will form, the governing equations can be presented in terms of a stream function. The following system of equations results

$$\frac{1}{Va}\frac{\partial}{\partial t}\left(\frac{\partial^2\Psi}{\partial x^2}+\frac{\partial^2\Psi}{\partial z^2}\right)+\left(\frac{\partial^2\Psi}{\partial x^2}+\frac{\partial^2\Psi}{\partial z^2}\right)=-Ra\frac{dt}{dx} \tag{3.1}$$

$$\frac{\partial T}{\partial t}+\frac{\partial\Psi}{\partial z}\frac{\partial T}{\partial x}-\frac{\partial\Psi}{\partial x}\frac{\partial T}{\partial z}=\frac{\partial^2 T}{\partial x^2}+\frac{\partial^2 T}{\partial z^2} \tag{3.2}$$

The Vadasz number is defined as

$$Va=\frac{\Phi Pr_D}{Da} \tag{3.3}$$

This number is typically very large due to $\Phi/_{Da}$ typically being on the order of 10 to 10^{20}. Because of this, the time derivative term was generally neglected. However, Vadasz and Olek [4], [9], [10] showed that this term should not be neglected when studying wave phenomena.

From this set of equations, a simplified set of equations can be derived by representing the stream and temperature functions (T and Ψ, respectively) in terms of a truncated Galerkin expansion, where A_{11}, B_{11}, and B_{02} represent the amplitudes of each term and are unknown and time dependent.

$$\Psi = A_{11}\, sin(\kappa_x x)\, sin(\kappa_z z) \tag{3.4}$$

$$T = 1 - z + B_{11}\, cos(\kappa_x x)\, sin(\kappa_z z) + B_{02}\, sin(2\kappa_z z) \tag{3.5}$$

κ_x and κ_z are the wave numbers of the convection in the x and z directions, respectively. These numbers are derived by examining the transition from the motionless solution to the convective solution. For the boundary conditions of the problem domain to be satisfied, ω_z must be in the form $\kappa_z = n\pi$, where $n = 1, 2, 3, ...$ κ_x must also be in the form $\kappa_x = m\pi$, where $m = 1, 2, 3, ...$ for the same reason. Linear stability analysis shows that at the critical Rayleigh number, Ra_{cr} perturbations of a certain wavenumber will grow exponentially, which causes the motionless solution to become unstable. The relationship between Ra_{cr} and κ_x is shown by linear stability analysis to be

$$Ra_{cr} = \kappa_x^2 + 2n\pi + \frac{m^4\pi^4}{\omega_x^2} \tag{3.6}$$

The motionless solution will become unstable at the minimum value for Ra_{cr} which occurs. Clearly this minimum will occur when $n = 1$, resulting in $\kappa_z = \pi$. The minimum value of equation (3.6) is found by taking the derivative with respect to κ_x and equating it to zero,

$$\frac{\partial Ra_c}{\partial_{\omega_x}^2} = 0 = \frac{(\kappa_x^2 + m^2\pi^2)[2\kappa_x^2 - (\kappa_x^2 + m^2\pi^2)]}{\kappa_x^2} \tag{3.7}$$

$$\Rightarrow \kappa_x^2 = \pi^2 \tag{3.8}$$

Figure 3.1 shows equation (3.6). The values which result in the minimum are shown in the plot as the critical Rayleigh number and the critical wavenumber, Ra_{cr} and κ_{cr}, respectively. When $Ra = Ra_{cr}$, the perturbations with the wavenumber $\kappa_{cr} = \pi$ will grow exponentially and cause

the motionless solution to become unstable. As a result, this value is called the critical wavenumber, κ_{cr}. Near the transition from the motionless solution to the convective solution this wavenumber dominates. As a result, the critical wavenumber is used in the derivation of the Lorenz system of equations. This assumption dictates that two convection cells will form for all Rayleigh numbers.

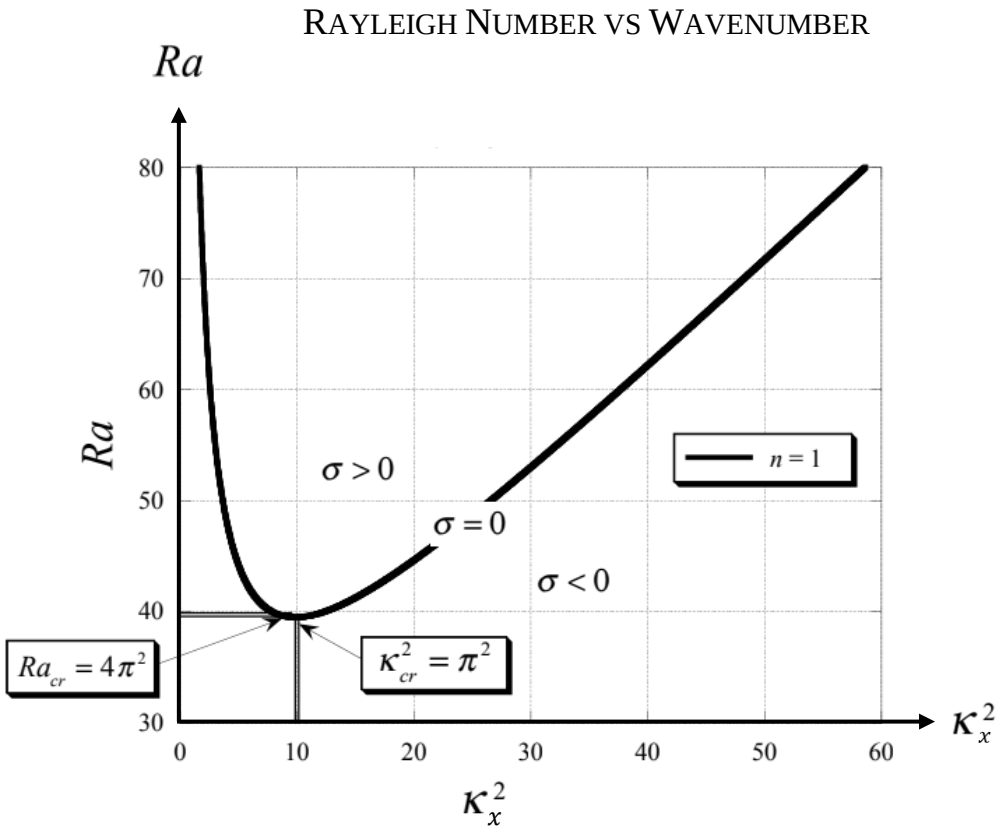

Figure 3.1: The relationship between the Rayleigh number and the critical wavenumber, derived using linear stability analysis. The minimum of this line is the point at which the motionless solution becomes unstable, and perturbations of wavenumber κ_{cr} grow exponentially. Graph used with permission [13].

Substituting the critical wavenumber for κ_x and κ_z into equations (3.4) and (3.5) results in the following system,

$$\Psi = A_{11}\, sin(\pi x)\, sin(\pi z) \tag{3.9}$$

$$T = 1 - z + B_{11}\, cos(\pi x)\, sin(\pi z) + B_{02}\, sin(2\pi z) \tag{3.10}$$

A_{11}, B_{11}, and B_{02} are found by substituting (3.9) and (3.10) into (3.1) and (3.2). After considerable simplification, the details of which are outlined in Vadasz and Olek [4], [9], [10] the following system of ordinary differential equations results

$$\frac{dA_{11}}{dt} = -\frac{Va}{2\pi^2}\left[A_{11} + \frac{Ra}{2\pi}B_{11}\right] \tag{3.11}$$

$$\frac{dB_{11}}{dt} = -B_{11} - \frac{1}{2\pi}A_{11} - \frac{1}{2}A_{11}B_{02} \tag{3.12}$$

$$\frac{dB_{02}}{dt} = -2B_{02} + \frac{1}{4}A_{11}B_{11} \tag{3.13}$$

The amplitude equations are rescaled relative to the critical Rayleigh number by making the following substitutions

$$R = \frac{Ra}{4\pi^2} \rightarrow Ra = 4\pi^2 R \tag{3.14}$$

$$\alpha = \frac{Va}{2\pi^2} \rightarrow Va = 2\pi^2 \alpha \tag{3.15}$$

The system of equations is additionally scaled relative to the fixed points, which can be found by setting the left hand side of equations (3.11), (3.12), and (3.13) equal to zero and solving for A_{11}, B_{11}, and B_{02}.

$$0 = -\frac{Va}{2\pi^2}\left[A_{11} + \frac{Ra}{2\pi}B_{11}\right] \tag{3.16}$$

$$0 = -B_{11} - \frac{1}{2\pi}A_{11} - \frac{1}{2}A_{11}B_{02} \tag{3.17}$$

$$0 = -2B_{02} + \frac{1}{4}A_{11}B_{11} \tag{3.18}$$

The fixed points are found to be

$$A_{11,f} = -4\sqrt{R-1} \tag{3.19}$$

$$B_{11,f} = \frac{2\sqrt{R-1}}{\pi R} \tag{3.20}$$

$$B_{02,f} = -\frac{R-1}{\pi R} \tag{3.21}$$

Equations (3.11), (3.12), and (3.13) are scaled relative to the fixed points by defining X, Y, and Z as follows

$$X = -\frac{A_{11}}{4\sqrt{R-1}} \rightarrow A_{11} = -4\sqrt{R-1}X \tag{3.22}$$

$$Y = \frac{\pi R B_{11}}{2\sqrt{R-1}} \rightarrow B_{11} = \frac{2\sqrt{R-1}}{\pi R}Y \tag{3.23}$$

$$Z = -\frac{\pi R}{R-1}B_{02} \rightarrow B_{02} = -\frac{R-1}{\pi R}Z \tag{3.24}$$

This re-scaling removes the explicit dependence on the fixed points so that the new convective fixed points are $X_f = \pm 1$, $Y_f = \pm 1$, and $Z_f = 1$. The final form of the ordinary differential equations is

$$\dot{X} = \alpha(Y - X) \tag{3.25}$$

$$\dot{Y} = -Y + RX - (R - 1)XZ \tag{3.26}$$

$$\dot{Z} = 2(XY - Z) \tag{3.27}$$

This system is equivalent to the Lorenz system of ordinary differential equations (with different coefficients) and is an approximation for (3.1) and (3.2).

This system has been solved computationally by Vadasz and Olek using Adomian's decomposition method in [4], [9], [14]–[19] and analytically using weak nonlinear analysis in [14], [16], [17], [19], [20]. These results (computational and analytical) have been used to study the transition from steady convection to chaos and have been shown to generally agree for Rayleigh numbers close to the transition point [19]. Analytical and numerical comparisons have not yet been made near the critical Rayleigh number.

Previous analysis of this system of equations focused on studying the transition to chaos for natural convection in porous media. However, the solution of these equations has not been compared to the solution of the original equations from which they were derived. As a result, the range of Rayleigh numbers for which the Lorenz equations agree with the original equations governing natural convection in porous media is not known.

4 METHODS

Experimental data analysis

Natural convection in porous media has been studied extensively in the laboratory, especially for the range of Rayleigh numbers $40 < Ra < 100$. A convenient overview of the experimental and theoretical work done on the topic was done by Cheng [2]. Investigation of the original publications compiled by Cheng revealed that two types of experimental setups were used in the experiments. Firstly, a rectangular domain, where the top and bottom boundaries were kept at a constant temperature, with insulated sides. Secondly, a cylindrical domain, with the outside of the cylinder insulated and the top and bottom kept at constant temperature.

The problem formulation describes a rectangular domain with top and bottom boundaries kept at constant temperatures and with insulated sides. As a result, the cylindrical experimental setup is not sufficiently close to that of the present numerical and Lorenz system problem domain and is not considered in this analysis. The resulting reduced data set contains data from two publications: Kaneko et al [6] and Combarnous and Bories [8]. The data was pulled from the plots of the original publications with a tool called ‘Data Thief III’ [21].

The original data set compiled by Cheng and the reduced data set both show a wide dispersion of data, indicating that the dispersion is likely not the result of dissimilar experimental setups. A theoretical explanation of this wide dispersion was presented by Vadasz [7]. By deriving an analytical relationship between the Nusselt number and the Rayleigh number via a weak nonlinear solution, Vadasz showed that the resulting system was extremely sensitive to the initial conditions and the boundary imperfections of the experimental setup, neither of which can be

predicted nor controlled. The upper and lower bounds on the weak nonlinear solution agree with the upper and lower bounds on the experimental data.

The reduced data set, which is used to compare the Nusselt numbers for the Lorenz system and numerical results with experimental data, is presented below in Figure 4.1. The details of the porous structure and saturating fluid for each experimental run are shown in Table 4-1.

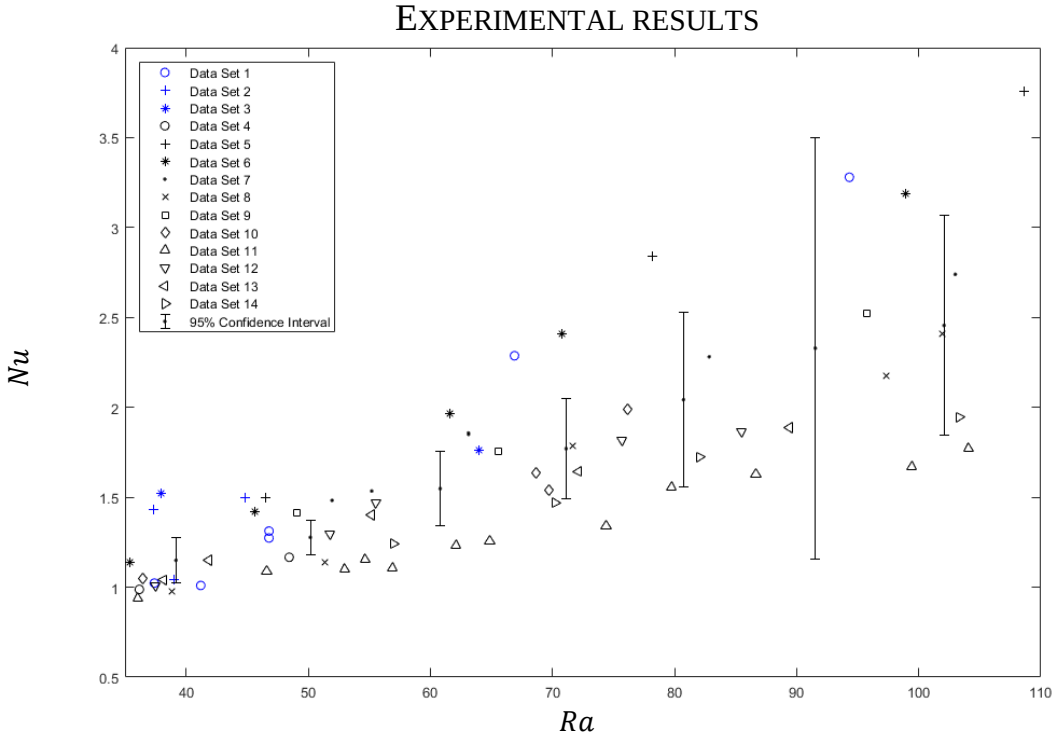

Figure 4.1: The raw experimental data for Nusselt vs. Rayleigh number with error bars representing a 95% confidence interval.

The error bars were calculated by dividing the data set into bins of length $Ra = 10$, with the bins centered at $Ra = 10, 20, 30, \ldots, 100$. The 95% confidence interval was used to calculate the error bars, and each bar is centered at the mean of the data at each bin.

Table 4-1: Experimental details of each data set from Figure 4.1.

	Author	**Porous structure**	**Saturating fluid**
Data Set 1	Kaneko et al	12/14 mesh sand	Heptane
Data Set 2		14/16 mesh sand	Ethanol
Data Set 3		12/14 mesh sand	
Data Set 4	Combarnous and Bories	Polypropylene beads, $D = 4mm$	Water
Data Set 5		Glass beads, $D = 2mm$	Oil
Data Set 6		Glass beads, $D = 0.9mm$	
Data Set 7		Glass beads, $D = 4mm$	Water
Data Set 8		Glass beads, $D = 3mm$	
Data Set 9		Glass beads, $D = 1.7mm$	
Data Set 10		Quartz sand, $D = 1.9mm$	Oil
Data Set 11		Quartz sand, $D = 1.9mm$	Water
Data Set 12		Quartz sand, $D = 2.25mm$	
Data Set 13		Quartz sand, $D = 2.25mm$	
Data Set 14		Lead balls, $D = 4mm$	

The experimental data indicates that for some trials natural convection occurred slightly before or after the theoretical transition point. An analytical explanation was presented by Vadasz and Braester [22]. Theoretically, when the side walls are perfectly insulated, the transition from the motionless solution to the convective solution occurs via a perfect pitchfork bifurcation. This means that the motionless solution becomes unstable and two stable solution branches emerge:

clockwise rotation or counterclockwise rotation of convection cells. The branch the solution proceeds down is determined by the initial conditions.

However, when there are small imperfections in the insulation of the sidewalls, resulting in heat leakage out of the sides, the nature of the transition from the motionless solution to the convective solution changes. The transition to the convective solution occurs via an imperfect bifurcation. Subcritical convection may occur, the nature of which is uniquely determined by the amount heat leakage from the sides of the problem domain and the resulting initial conditions of the problem.

Figure 4.2 presents graphically the distinction between the perfect pitchfork bifurcation and the imperfect bifurcation. Inspection of the imperfect bifurcation diagram shows that low amplitude sub-critical convection occurs when there is heat leakage through the walls. Close to the transition point, these imperfections result in larger amplitude convection than occurs when there are no imperfections. As the Rayleigh number increases, the amplitude of the convection that occurs when there is heat leakage approaches that which occurs when there are no imperfections.

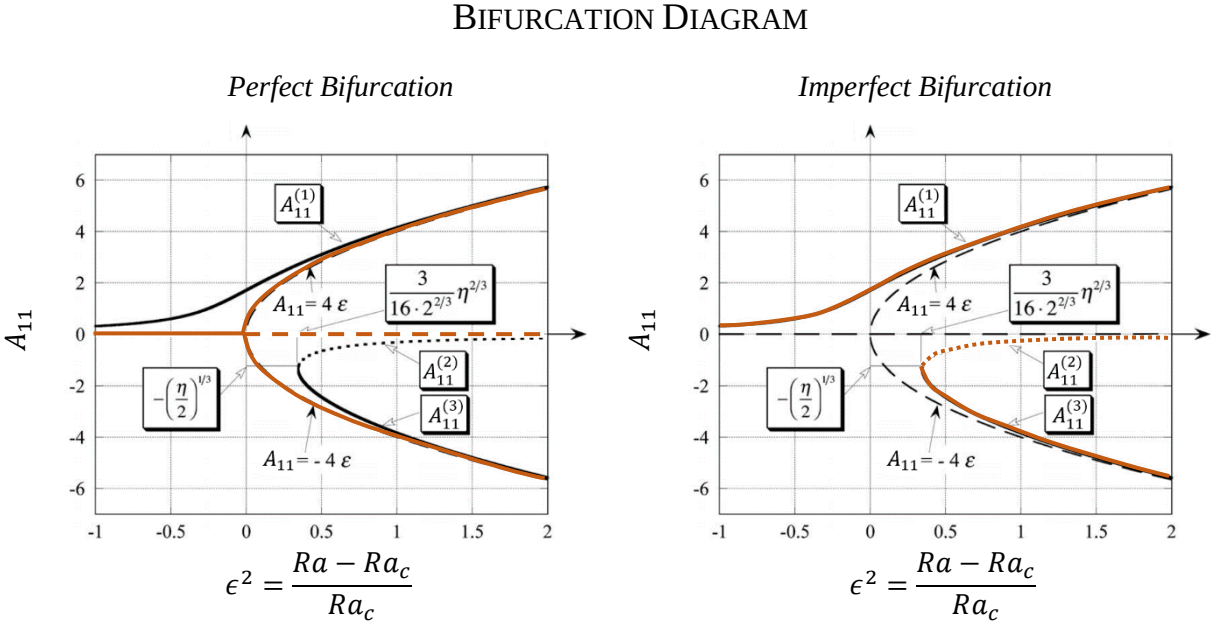

Figure 4.2: The bifurcation diagram shows a perfect bifurcation on the left, which occurs when there are no imperfections in the boundary conditions, and an imperfect bifurcation on the right, which occurs when there is heat leakage through the walls. The boundary imperfections are represented by the parameter η. An increase in η represents an increase in the boundary imperfections. Graph used with permission from [7].

In practice, it is impossible to perfectly insulate the sidewalls of an experimental setup. The result is that the experimental transition to convection may occur before Ra_{cr}.

Solution of Lorenz system

The Lorenz system to be solved was derived in Chapter 3 from equations (3.1) and (3.2).This system is equivalent to the Lorenz equations, which are a simplified model for atmospheric natural convection [5], [18].

$$\dot{X} = \alpha(Y - X) \tag{4.1}$$

$$\dot{Y} = -Y + RX - (R - 1)XZ \tag{4.2}$$

$$\dot{Z} = 2(XY - Z) \tag{4.3}$$

$\dot{X}$, $\dot{Y}$, and $\dot{Z}$ represent the amplitude equations for the coefficients of the truncated Galerkin expansion of the governing equations. For the purpose of this research the solutions for X, Y, and Z were found using an explicit Runge-Kutta scheme. The results were then rescaled to their original form using,

$$X = -\frac{A_{11}}{4\sqrt{R-1}} \rightarrow A_{11} = -4\sqrt{R-1}X \tag{4.4}$$

$$Y = \frac{\pi R B_{11}}{2\sqrt{R-1}} \rightarrow B_{11} = \frac{2\sqrt{R-1}}{\pi R}Y \tag{4.5}$$

$$Z = -\frac{\pi R}{R-1}B_{02} \rightarrow B_{02} = -\frac{R-1}{\pi R}Z \tag{4.6}$$

$$R = \frac{Ra}{4\pi^2} \rightarrow Ra = 4\pi^2 R \tag{4.7}$$

$$\alpha = \frac{Va}{2\pi^2} \rightarrow Va = 2\pi^2 \alpha \tag{4.8}$$

The results for A_{11}, B_{11}, and B_{02} are then substituted back into equations (3.9) and (3.10).

The final results for stream function and temperature are calculated for every point in the problem domain using a mesh of x and z coordinates. The mesh is chosen so that the grid points from the Lorenz system line up with the grid points from the numerical solution. This allows for a direct comparison to be made without the need for interpolation.

Numerical

The numerical method chosen for the purposes of this research is a direct numerical simulation of the governing equations. The stream function and temperature functions are discretized using a fully implicit finite difference scheme with a single in space to deal with the nonlinearity and coupling between temperature and the stream function. Chapter 5 presents the details of the numerical method of solution.

5 NUMERICAL METHOD OF SOLUTION

Overview

The governing equations are discretized using a fully implicit finite difference scheme. The problem domain is broken into a uniform spatial mesh so $\Delta x = \Delta z = \Delta L$. The governing equations are time dependent, and each time step forward in time is represented by a constant Δt.

The two governing equations are nonlinear and coupled and thus cannot be solved independent of each other. The numerical method uses an iterative method to find a solution for both temperature and stream functions which satisfies both equations.

Discretization of governing equations

Figure 5.1 below shows the details of the single index spatial mesh used to discretize the problem domain. At each point, i, the temperature and stream values are unknown, and at each point the governing equations are discretized to represent the heat transfer and fluid flow. The result is a system of $2(M \cdot N)$ linear equations with $2(M \cdot N)$ unknowns, since the values of both the stream function and temperature are unknown.

The system is solved first for the values of temperature at each point and then for the values of the stream function, using an iterative method. Initially, the values of the previous time step are being used for the solution of the energy equation. The resulting values of T are then used to solve for the new values of Ψ. This procedure is repeated until no change beyond a set tolerance occurs. This method means that only an $M \cdot N$ matrix system must be solved at each time step time instead of a $2(M \cdot N)$ matrix system.

DISCRETIZATION SCHEME

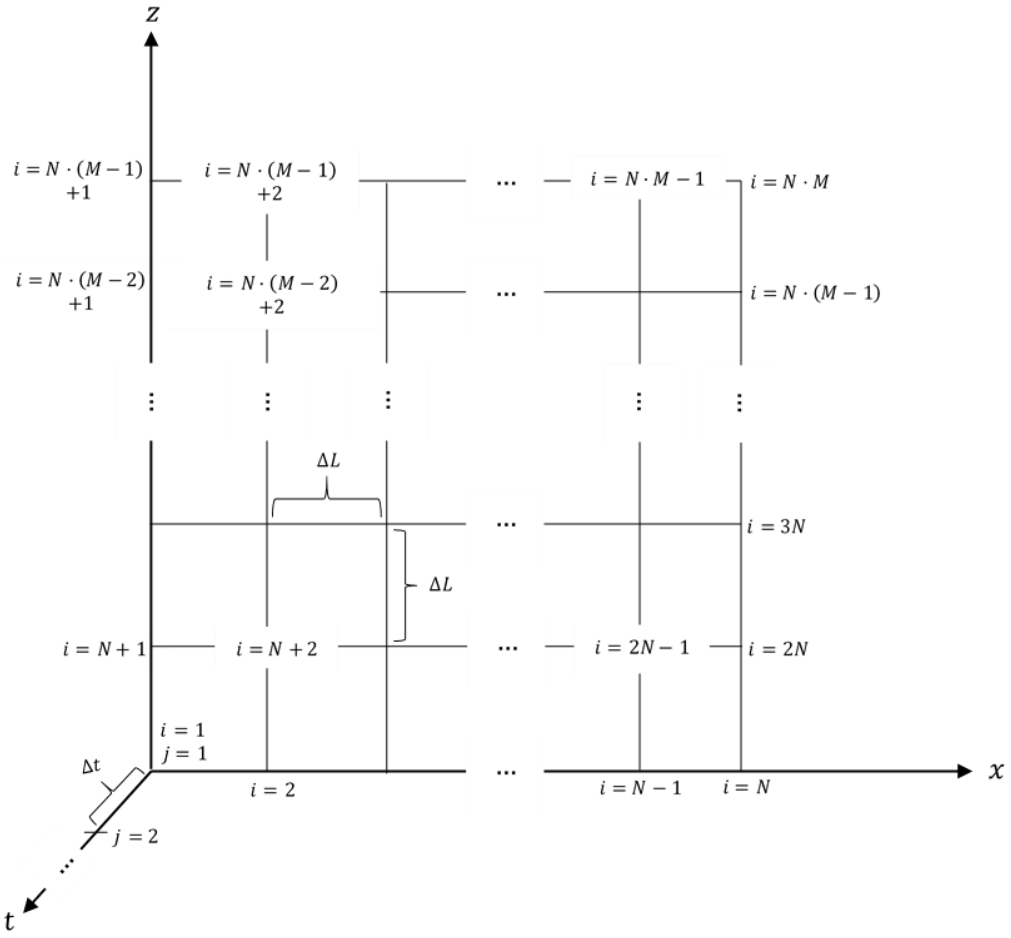

Figure 5.1: Discretization scheme for problem domain.

The domain is broken into $N-1$ sub-grids for a total of N grid points in the $x-$direction. Similarly, in the $z-$direction the domain is broken into $M-1$ sub-grids for a total of M grid points. Each spatial grid point has an index denoted by i, totaling $M \cdot N$ grid points. When the governing equations are discretized, they will be a set of $M \cdot N$ equations with the value at each grid point being an unknown. This linear system is solved to find the solution to the linear system at each point. The system is also time dependent. The index j represents the point in time at which the linear system is solved. The discretization scheme is represented graphically in Figure 5.1.

Temperature Function

$$\frac{\partial T}{\partial t}+\frac{\partial \psi}{\partial z}\frac{\partial T}{\partial x}-\frac{\partial \Psi}{\partial x}\frac{\partial T}{\partial z}=\frac{\partial^2 T}{\partial x^2}+\frac{\partial^2 T}{\partial z^2} \tag{5.1}$$

Equation (5.1) above is the simplified equation for conservation of energy, with the stream function and 2D flow simplification applied. This equation is discretized using a forward difference scheme in time and a centered difference scheme in space. Equation (5.1) is coupled with equation (5.6) below because both equations have Ψ and T as dependent variables. Equations (5.2) through (5.4) are the discretized form of (5.1).

$$\frac{T_i^{j+1}-T_i^j}{\Delta t}+u_i\frac{T_{i+1}^{j+1}-T_{i-1}^{j+1}}{2\Delta L}+w_i\frac{T_{i+N}^{j+1}-T_{i-N}^{j+1}}{2\Delta L} = \frac{T_{i-1}^{j+1}-2T_i^{j+1}+T_{i+1}^{j+1}}{\Delta L^2}+\frac{T_{i-N}^{j+1}-2T_i^{j+1}+T_{i+N}^{j+1}}{\Delta L^2} \tag{5.2}$$

Where,

$$u_i=\frac{\Psi_{i+N}-\Psi_{i-N}}{2\Delta L} \tag{5.3}$$

$$w_i=-\frac{\Psi_{i+1}-\Psi_{i-1}}{2\Delta L} \tag{5.4}$$

Equation (5.5) below expresses the known temperature values on the left-hand side and the unknown temperature values on the right-hand side with known coefficients.

$$T_i^j = \left(u_i \frac{\Delta t}{2\Delta L} - \frac{\Delta t}{\Delta L^2}\right) T_{i+1}^{j+1} - \left(u_i \frac{\Delta t}{2\Delta L} + \frac{\Delta t}{\Delta L^2}\right) T_{i-1}^{j+1} + \left(w_i \frac{\Delta t}{2\Delta L} - \frac{\Delta t}{\Delta L^2}\right) T_{i+N}^{j+1} - \left(w_i \frac{\Delta t}{\Delta L^2} + \frac{\Delta t}{2\Delta L}\right) T_{i-N}^{j+1} + \left(\frac{4\Delta t}{\Delta L^2} + 1\right) T_i^{j+1} \tag{5.5}$$

Stream Function

$$\frac{1}{Va}\frac{\partial}{\partial t}\left(\frac{\partial^2 \Psi}{\partial x^2} + \frac{\partial^2 \Psi}{\partial z^2}\right) + \left(\frac{\partial^2 \Psi}{\partial x^2} + \frac{\partial^2 \Psi}{\partial z^2}\right) = -Ra\frac{dT}{dx} \tag{5.6}$$

Equation (5.6) above is the simplified equation for conservation of momentum, extended Darcy's law, with the stream and 2D flow simplification applied. This is discretized in the same way as equation (5.1) using a forward difference scheme in time and a centered difference scheme in space. Equation (5.7) is the discretized form of (5.6)(5.8).

$$\frac{1}{Va}\frac{1}{\Delta t}\left[\left(\frac{\Psi_{i-1}^{j+1} - 2\Psi_i^{j+1} + \Psi_{i+1}^{j+1}}{\Delta L^2} + \frac{\Psi_{i-N}^{j+1} - 2\Psi_i^{j+1} + \Psi_{i+N}^{j+1}}{\Delta L^2}\right) - \left(\frac{\Psi_{i-1}^{j} - 2\Psi_i^{j} + \Psi_{i+1}^{j}}{\Delta L^2} + \frac{\Psi_{i-N}^{j} - 2\Psi_i^{j} + \Psi_{i+N}^{j}}{\Delta L^2}\right)\right] + \left(\frac{\Psi_{i-1}^{j+1} - 2\Psi_i^{j+1} + \Psi_{i+1}^{j+1}}{\Delta L^2} + \frac{\Psi_{i-N}^{j+1} - 2\Psi_i^{j+1} + \Psi_{i+N}^{j+1}}{\Delta L^2}\right) = -Ra\frac{T_{i-1}^{j+1} - T_{i+1}^{j+1}}{2\Delta L} \tag{5.7}$$

Equation (5.8) below expresses the known temperature values on the left-hand side and the unknown temperature values on the right-hand side with known coefficients.

$$
\begin{aligned}
&(Va\Delta t + 1)\left(\Psi_{i-N}^{j+1} + \Psi_{i-1}^{j+1} - 4\Psi_i^{j+1} + \Psi_{i+1}^{j+1} + \Psi_{i+N}^{j+1}\right) \\
&\quad = -\frac{RaVa\Delta t\Delta L}{2}\left(T_{i-1}^{j+1} - T_{i+1}^{j+1}\right) \\
&\quad + \left(\Psi_{i-N}^{j} + \Psi_{i-1}^{j} - 4\Psi_i^{j} + \Psi_{i+1}^{j} + \Psi_{i+N}^{j}\right)
\end{aligned}
\tag{5.8}
$$

Boundary conditions

Equations (5.8) and (5.5) represent the discretized equations for all grid points in the problem domain, with the exception of the boundaries.

$x = 0$:

$$\Psi^{j+1} = \Psi^{j} = 0 \tag{5.9}$$

$$
\begin{aligned}
T_i^j = &-\left(\frac{\Delta t}{\Delta L^2}\right) T_{i-N}^{j+1} - 2\left(\frac{\Delta t}{\Delta L^2}\right) T_{i-1}^{j+1} \\
&+ \left(\frac{4\Delta t}{\Delta L^2} + 1\right) T_i^{j+1} - \left(\frac{\Delta t}{\Delta L^2}\right) T_{i+N}^{j+1}
\end{aligned}
\tag{5.10}
$$

$x = L$:

$$\Psi^{j+1} = \Psi^{j} = 0 \tag{5.11}$$

$$
\begin{aligned}
T_i^j = &-\left(\frac{\Delta t}{\Delta L^2}\right) T_{i-N}^{j+1} - 2\left(\frac{\Delta t}{\Delta L^2}\right) T_{i-1}^{j+1} \\
&+ \left(\frac{4\Delta t}{\Delta L^2} + 1\right) T_i^{j+1} - \left(\frac{\Delta t}{\Delta L^2}\right) T_{i+N}^{j+1}
\end{aligned}
\tag{5.12}
$$

$z = 0$:

$$\Psi^{j+1} = \Psi^{j} = 0 \tag{5.13}$$

$$T^{j+1} = T^{j} = 1 \tag{5.14}$$

$z = 1$:

$$\Psi^{j+1} = \Psi^{j} = 0 \tag{5.15}$$

$$T^{j+1} = T^{j} = 0 \tag{5.16}$$

Iterative method of solution

Inspection of equations (5.5) and (5.6) shows that the two equations are coupled and cannot be solved independent of each other. Instead of solving the two equations simultaneously, which would be computationally intensive, an iterative method is applied. The values from the previous time step are used as a guess for the current time step. The solver iterates between the temperature solver and the stream function solver, using the latest solution as a guess for the next. When the solver has converged on a solution for the temperature and stream function values, the solver moves on to the next time step.

This process repeats until a steady state solution is reached, or until it is obvious that a steady state solution does not exist. The details of the iterative solution can be found in Figure 5.2 below.

SOLVER ALGORITHM

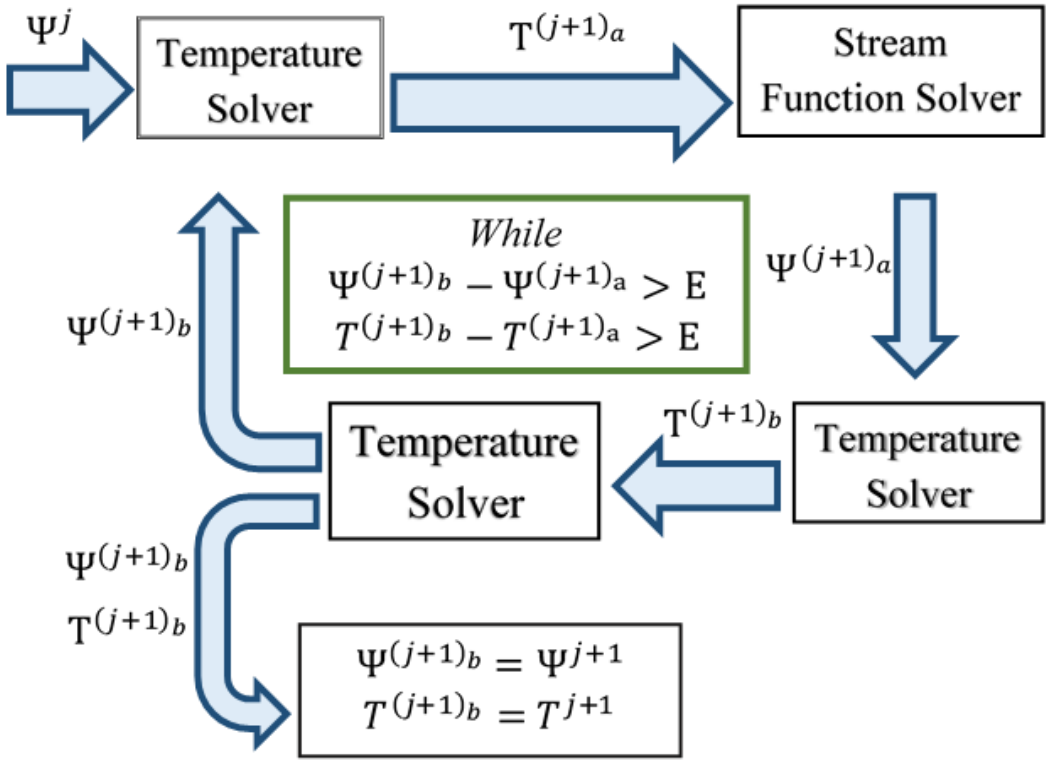

Figure 5.2: The detailed algorithm used for the numerical solver.

Figure 5.2 above shows the details of the iterative method used to solve the discretized form of the two governing equations. The index j represents the previous time step, at which all the values for temperature and stream function have been solved for to sufficient accuracy. Therefore, all values with this index represent known values. The values with the index $j + 1$ are unknowns. To solve for stream and temperature at the current time step (the $j + 1^{th}$ time step) the values for the stream function from the previous time step are used to compute a guess for temperature at the current time step. The resulting temperature values, which have index $(j + 1)_a$ in the figure above, are used to compute a guess for the stream values. This updated guess for the stream function, which have index $(j + 1)_b$ in the diagram is used to compute an updated guess for temperature. This iterative cycle continues, and the computed guesses converge to the true values for temperature and stream at the current time step. Once these values

for stream function and temperature converge to within a small chosen tolerance the solution is complete for that time step and the cycle begins again for the next time step.

Code verification

Overview

The numerical method of solution consists of many different interconnected parts, so there are many opportunities for errors to arise in the coding process. To ensure that there are no errors in the code a technique called the Method of Manufactured Solutions [23], [24] is used to verify the integrity of the custom solver.

To implement the Method of Manufactured solutions, a source term is added to the original discretized equations, which modifies the solver so that it is solving for a known solution instead of an unknown solution. The known solutions for temperature and stream are T_{MS} and Ψ_{MS}, respectively. These are chosen based on the initial and boundary conditions of the solver and are known as the "Manufactured Solutions". Once the manufactured solutions are chosen the source terms can be calculated. The procedure for modifying the governing equations is outlined below. Q_T is the source term for the temperature equation, and Q_Ψ is the source term for the stream equation.

Temperature:

$$\frac{\partial T_{MS}}{\partial t} + \frac{\partial \psi_{MS}}{\partial z}\frac{\partial T_{MS}}{\partial x} - \frac{\partial \Psi_{MS}}{\partial x}\frac{\partial T_{MS}}{\partial z} = \frac{\partial^2 T_{MS}}{\partial x^2} + \frac{\partial^2 T_{MS}}{\partial z^2} + Q_T \qquad (5.17)$$

Equation (5.17) is discretized using exactly the same scheme as equation (5.5) above,

$$\frac{T_{MS_i}^{j+1} - T_{MS_i}^{j}}{\Delta t} + u_i \frac{T_{MS_{i+1}}^{j+1} - T_{MS_{i-1}}^{j+1}}{2\Delta L} + w_i \frac{T_{MS_{i+N}}^{j+1} - T_{MS_{i-N}}^{j+1}}{2\Delta L}$$

$$= \frac{T_{MS_{i-1}}^{j+1} - 2T_{MS_i}^{j+1} + T_{MS_{i+1}}^{j+1}}{\Delta L^2} + \frac{T_{MS_{i-N}}^{j+1} - 2T_{MS_i}^{j+1} + T_{MS_{i+N}}^{j+1}}{\Delta L^2} \qquad (5.18)$$

$$+ Q_T$$

When the known values are gathered on the right-hand side and the unknown values on the left, equation (5.18) becomes,

$$T_{MS_i}^{j} = \left(u_i \frac{\Delta t}{2\Delta L} - \frac{\Delta t}{\Delta L^2}\right) T_{MS_{i+1}}^{j+1} - \left(u_i \frac{\Delta t}{2\Delta L} + \frac{\Delta t}{\Delta L^2}\right) T_{i-1}^{j+1}$$

$$+ \left(w_i \frac{\Delta t}{2\Delta L} - \frac{\Delta t}{\Delta L^2}\right) T_{MS_{i+N}}^{j+1} - \left(w_i \frac{\Delta t}{\Delta L^2} + \frac{\Delta t}{2\Delta L}\right) T_{MS_{i-N}}^{j+1} \qquad (5.19)$$

$$+ \left(\frac{4\Delta t}{\Delta L^2} + 1\right) T_{MS_i}^{j+1} + Q_T \cdot \Delta t$$

Stream Function:

$$\frac{1}{Va} \frac{\partial}{\partial t} \left(\frac{\partial^2 \Psi_{MS}}{\partial x^2} + \frac{\partial^2 \Psi_{MS}}{\partial z^2}\right) + \left(\frac{\partial^2 \Psi_{MS}}{\partial x^2} + \frac{\partial^2 \Psi_{MS}}{\partial z^2}\right) = -Ra \frac{dT_{MS}}{dx} + Q_\Psi \qquad (5.20)$$

Equation (5.20) is discretized using exactly the same scheme as equation (5.7) above,

$$\frac{1}{Va}\frac{1}{\Delta t}\left[\left(\frac{\Psi_{MS_{i-1}}^{j+1}-2\Psi_{MS_i}^{j+1}+\Psi_{MS_{i+1}}^{j+1}}{\Delta L^2}+\frac{\Psi_{MS_{i-N}}^{j+1}-2\Psi_{MS_i}^{j+1}+\Psi_{MS_{i+N}}^{j+1}}{\Delta L^2}\right)\right.$$
$$\left.-\left(\frac{\Psi_{MS_{i-1}}^{j}-2\Psi_{MS_i}^{j}+\Psi_{MS_{i+1}}^{j}}{\Delta L^2}+\frac{\Psi_{MS_{i-N}}^{j}-2\Psi_{MS_i}^{j}+\Psi_{MS_{i+N}}^{j}}{\Delta L^2}\right)\right]$$
$$+\left(\frac{\Psi_{MS_{i-1}}^{j+1}-2\Psi_{MS_i}^{j+1}+\Psi_{MS_{i+1}}^{j+1}}{\Delta L^2}\right.$$
$$\left.+\frac{\Psi_{MS_{i-N}}^{j+1}-2\Psi_{MS_i}^{j+1}+\Psi_{MS_{i+N}}^{j+1}}{\Delta L^2}\right)=-Ra\frac{T_{MS_i}^{j+1}-T_{MS_i}^{j}}{\Delta t}+Q_\Psi \tag{5.21}$$

Gathering the known values on the right and unknown values on the left, equation (5.21) becomes,

$$(Va\Delta t+1)\left(\Psi_{MS_{i-N}}^{j+1}+\Psi_{MS_{i-1}}^{j+1}-4\Psi_{MS_i}^{j+1}+\Psi_{MS_{i+1}}^{j+1}+\Psi_{MS_{i+N}}^{j+1}\right)$$
$$=-\frac{RaVa\Delta t\Delta L}{2}\left(T_{MS_{i-1}}^{j+1}-T_{MS_{i+1}}^{j+1}\right)$$
$$+\left(\Psi_{MS_{i-N}}^{j}+\Psi_{MS_{i-1}}^{j}-4\Psi_{MS_i}^{j}+\Psi_{MS_{i+1}}^{j}+\Psi_{MS_{i+N}}^{j}\right)+Q_\Psi$$
$$\cdot\left(Va\Delta t\Delta L^2\right) \tag{5.22}$$

Note that the source term must be added to the original discretized equations, before any gathering of terms or simplification is done.

Choosing an appropriate manufactured solution

The only restrictions on the manufactured solutions chosen are that they must be infinitely differentiable, they must be able to test all the pieces of the solver, and they must agree with the boundary conditions implemented, so that the solver can be thoroughly tested. Since the system

of equations being solved is dependent upon x,z, and t, the manufactured solutions used must also vary in those dimensions. The equations chosen are,

$$T_{MS} = (1 - e^{-t}) \cdot cos(\pi x) \cdot sin(\pi z) \tag{5.23}$$

$$\Psi_{MS} = (1 - e^{-t}) \cdot sin(\pi x) \cdot sin(\pi z) \tag{5.24}$$

These equations satisfy the initial conditions, and the boundary conditions can be made to agree with a slight modification in the original solver. Additionally, the manufactured solutions converge to a steady state solution because of the term $(1 - e^{-t})$. This means that the original solver needs no modification beyond adding the appropriate source terms and modification of the $T = 1$ boundary condition to $T = 0$.

Calculating the source term

The source terms are calculated as follows,

$$Q_T = \frac{\partial T_{MS}}{\partial t} + \frac{\partial \Psi_{MS}}{\partial z}\frac{\partial T_{MS}}{\partial x} - \frac{\partial \Psi_{MS}}{\partial x}\frac{\partial T_{MS}}{\partial z} - \frac{\partial^2 T_{MS}}{\partial x^2} - \frac{\partial^2 T_{MS}}{\partial z^2} \tag{5.25}$$

$$Q_\Psi = \frac{1}{Va}\frac{\partial}{\partial t}\left(\frac{\partial^2 \Psi_{MS}}{\partial x^2} + \frac{\partial^2 \Psi_{MS}}{\partial z^2}\right) + \left(\frac{\partial^2 \Psi_{MS}}{\partial x^2} + \frac{\partial^2 \Psi_{MS}}{\partial z^2}\right) + Ra\frac{dT_{MS}}{dx} \tag{5.26}$$

Since T_{MS} and Ψ_{MS} are known (equations (5.23) and (5.24)), the source terms are evaluated analytically by taking the appropriate derivatives. This is done using a symbolic solver to eliminate the possibility of human error.

The analytical expressions for the source terms are evaluated at each point in the problem domain and added to the known terms in the solver, as shown in equations (5.19) and (5.22). If

the terms in the original discretized equations are re-arranged or simplified in any way, the source term must be appropriately modified. This is why the source terms in equations (5.19) and (5.22) have coefficients. Since the governing equations are time dependent, a new set of source terms are evaluated for each time step.

Results

The solver was used to evaluate the modified system of equations for successively finer grids. As the grid is refined, the solution produced by the solver approaches the manufactured solution, which is calculated analytically. Figure 5.3 below shows the contour plots for the chosen manufactured solutions, T_{MS} and Ψ_{MS}. To show that the numerical solution is converging to the true solution, and thus show that the numerical solver has no errors, the numerical convergence is shown for four points in the problem domain in Figure 5.4.

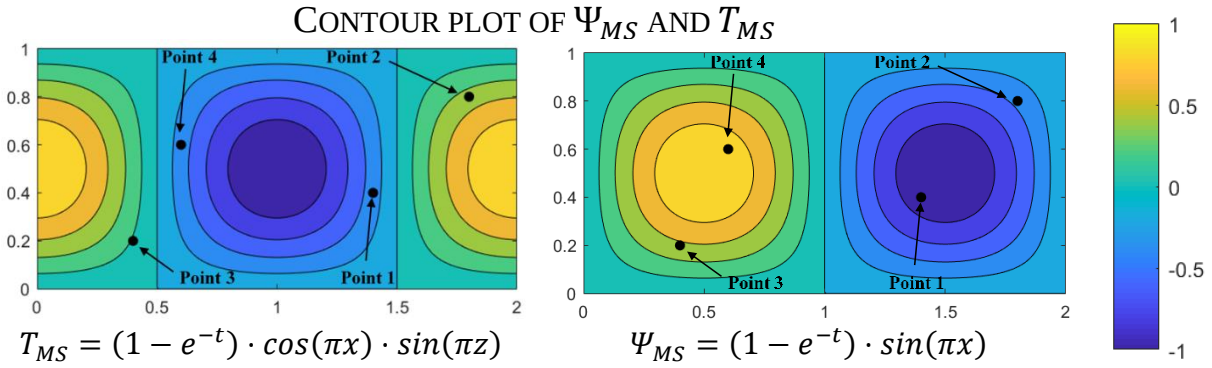

Figure 5.3: Contour plots of the manufactured solutions for temperature and stream. At each of the labeled points, the numerical value at that point is compared to the analytical value for increasingly fine meshes. This comparison is shown in Figure 5.4.

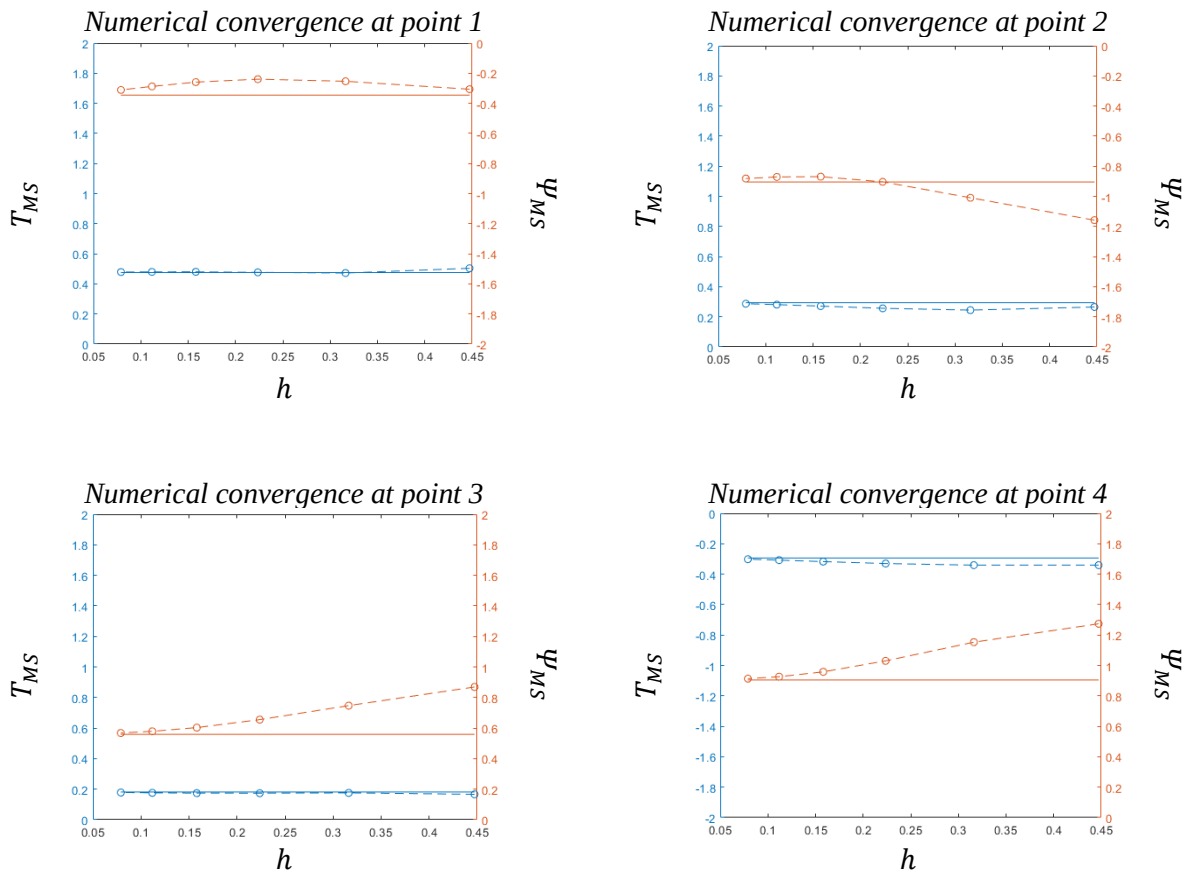

Figure 5.4: The numerical manufactured solution at 4 points for increasingly fine meshes and compared to the analytical manufactured solution. In the figures above, $h = \sqrt{L/N}$, where L is the length of the problem domain in the x-direction (in this case $L = 2$), and N is the number of computational nodes along that length. Consequently, decreasing h represents finer meshes.

Conclusion

The results above show that the as the grid is refined the output from the solver approaches the true solution. This means that the solver is free of coding errors and is solving the intended equations.

6 RESULTS AND DISCUSSION

Results

The solver was used to produce results on grids from 50 by 25 nodes up to 800 by 400 nodes. The results for the finest meshes are presented below. The solver was ran for Rayleigh numbers by increments of 10, beginning at $Ra = 40$, which is just above the critical Rayleigh number, up to $Ra = 100$. This range of Rayleigh numbers was chosen due to the availability of experimental data and due to the long length of time needed to run the solver to completion for sufficiently fine meshes when the Rayleigh number is greater than $Ra = 100$.

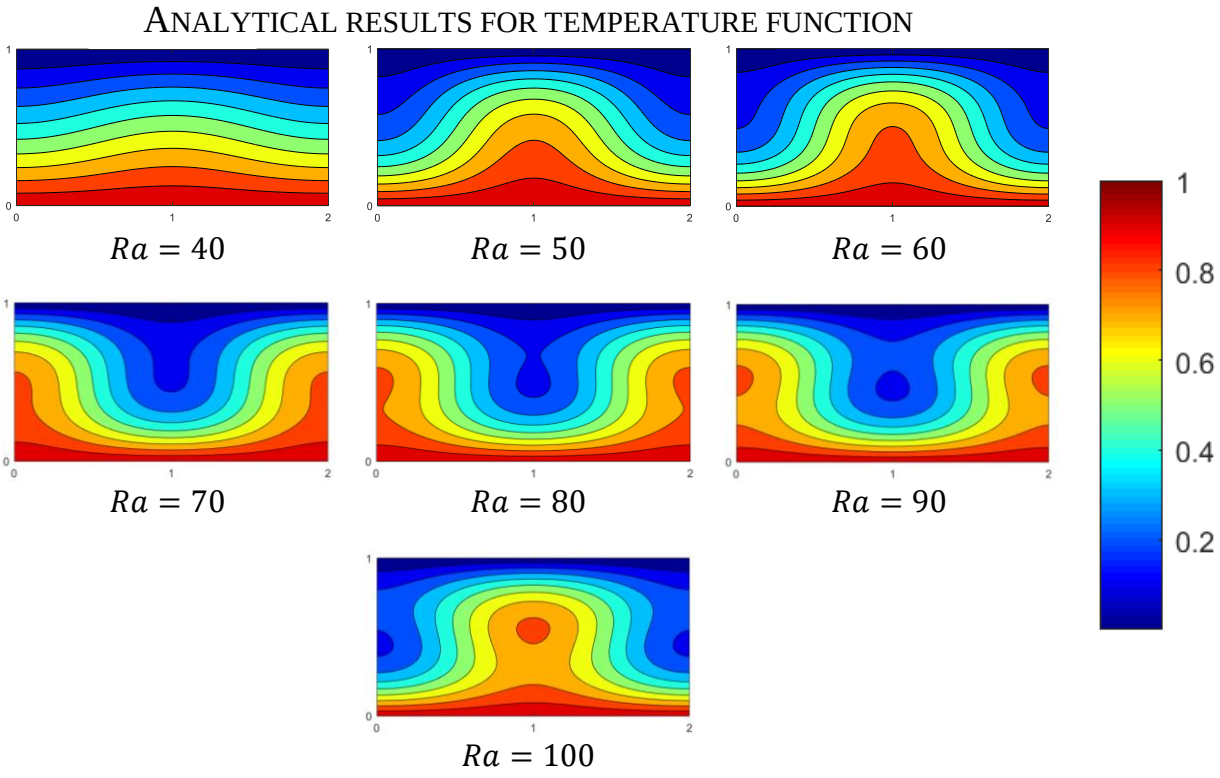

Figure 6.1: The results for temperature from the Lorenz system. The color contours represent the magnitude of the stream function and are scaled from 0 to 1, since $T = 1$ is the maximum temperature that can occur.

Figure 6.1 above shows the results for the temperature from the Lorenz system. The convection cells may form such that the fluid rises from the center of the problem domain, or they may form such that the fluid rises at the edges of the problem domain. For the purposes of discussion these two solutions are referred to the two solution branches. The resultant branch is dependent on the initial conditions of the problem. The Lorenz system will always produce two convection cells for a domain having an aspect ratio of $L = 2$. The Lorenz system also assumes that longitudinal rolls will prevail as the final nature of the solution.

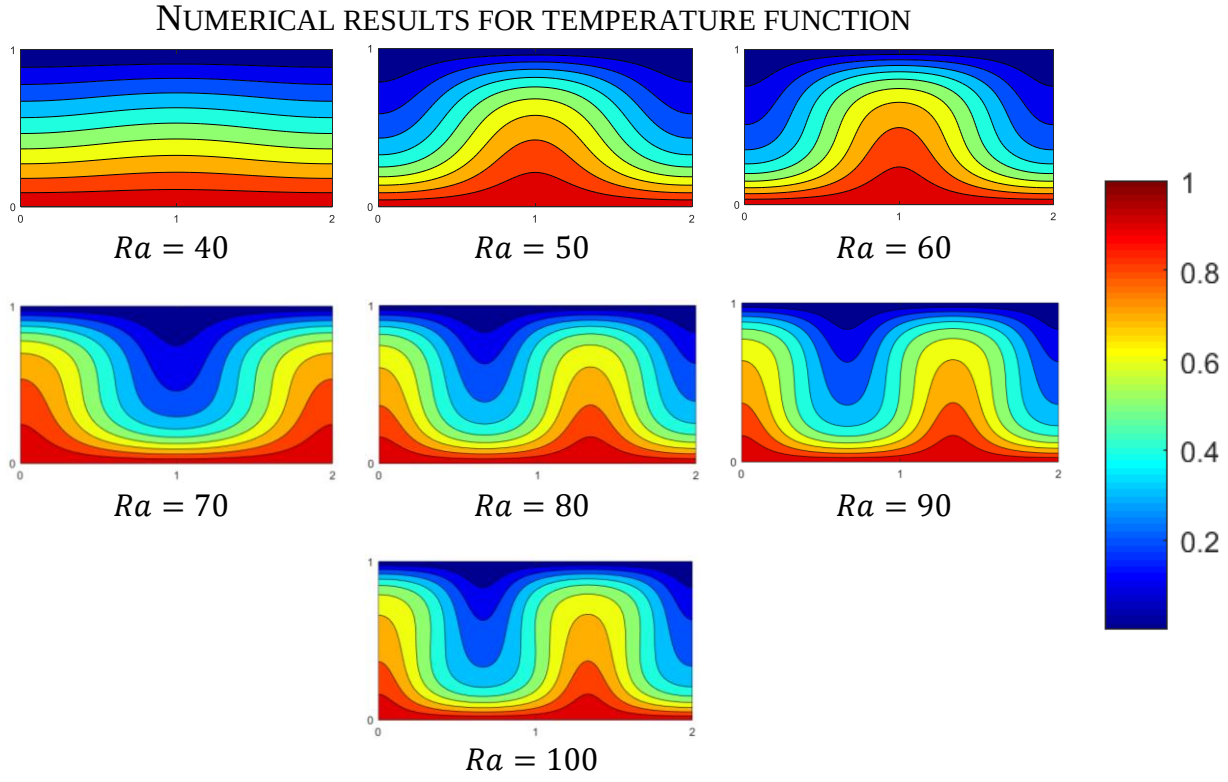

Figure 6.2: The results for temperature from the numerical solution. The color contours represent the magnitude of the temperature and are scaled from 0 to 1, since $T = 1$ is the maximum temperature that can occur.

Figure 6.1 above shows the results for temperature from the numerical solver. The numerical solution can result in the same two branches as the Lorenz system, with the fluid rising from the

center or the sides. The numerical solution also assumes that 2D longitudinal cells is the resulting convective cell pattern, but does not assume that two convection cells will result. Instead, the solver is left without any constraint on the number of convection cells that will occur. The wavenumber is a result of the numerical solution instead of being chosen, as in the Lorenz system. For Rayleigh numbers $Ra \geq 80$ the numerical solution predicts that more than 2 convection cells will occur.

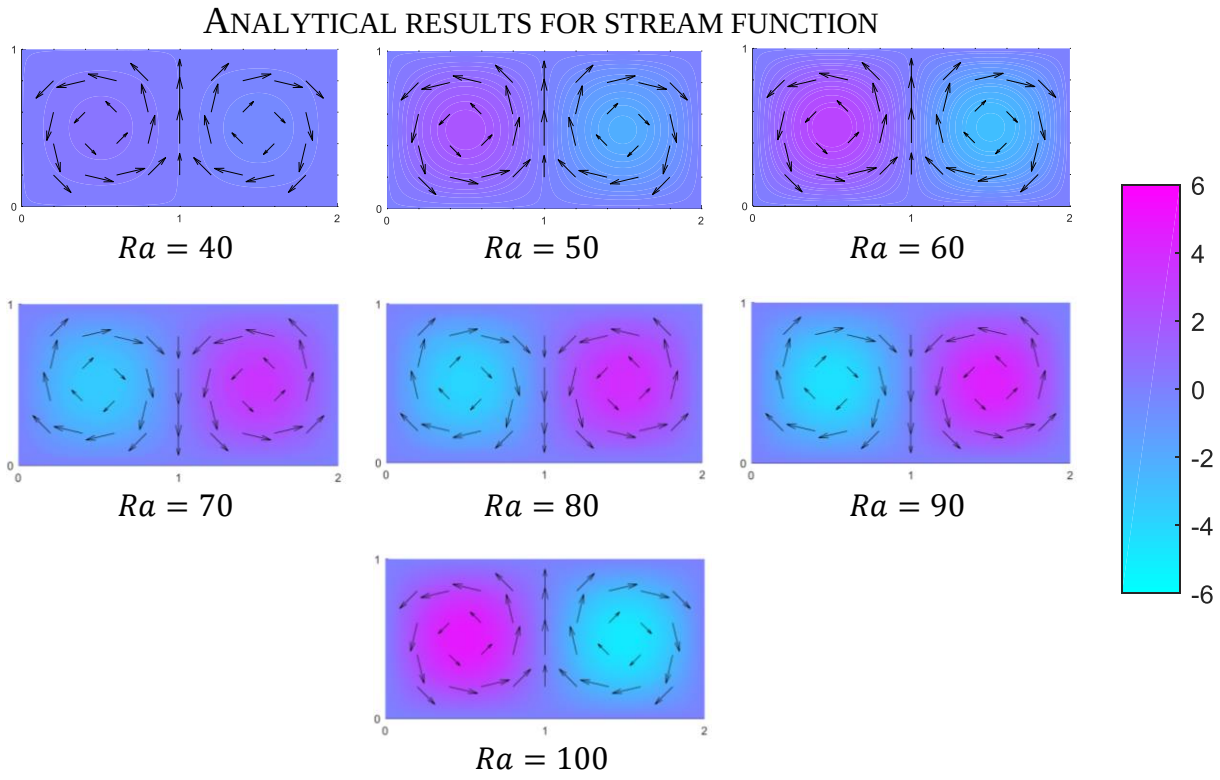

Figure 6.3: The results for the stream function from the Lorenz system. The color contours represent the magnitude of the stream function and are scaled from -6 to 6 for ease of comparison. The arrows show the direction of the flow.

Figure 6.3 above shows the results for the stream function from the Lorenz system. The results for the stream function provide insight as to why the two solution branches occur. The two

branches are identical except that the clockwise-rotation convection cell can occur on the right side of the problem domain or the left, depending on the initial conditions.

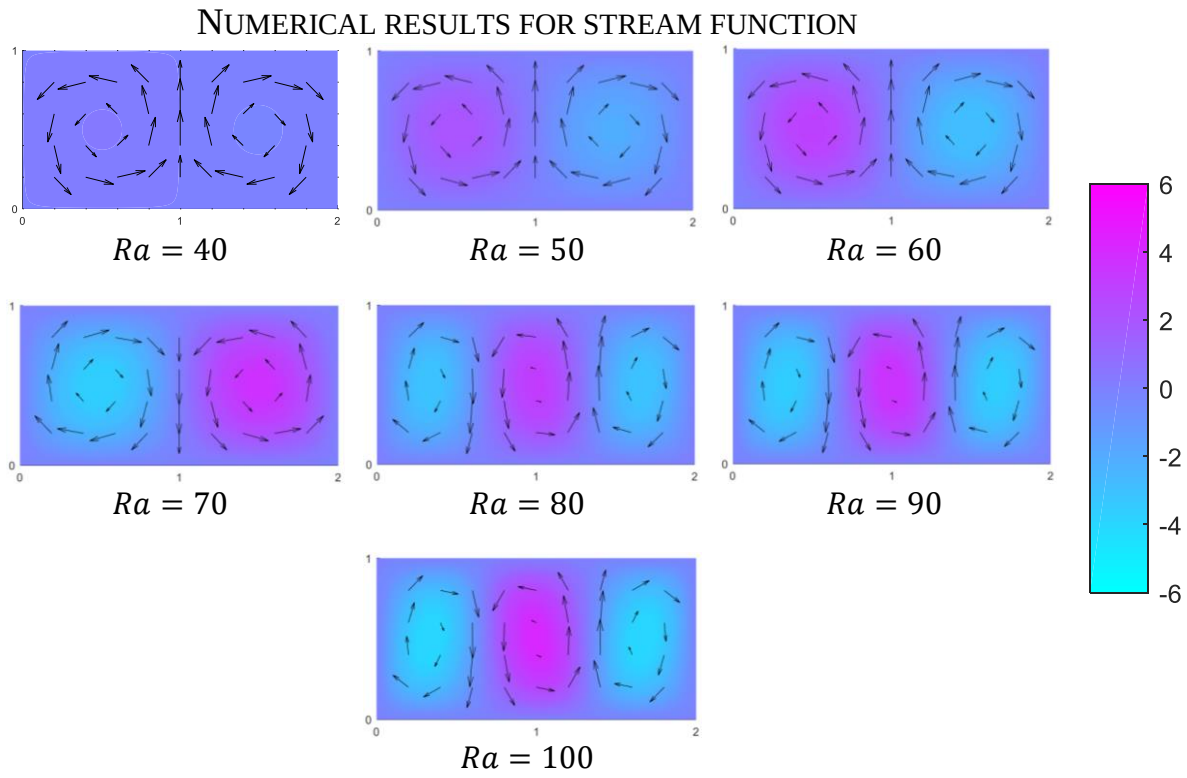

Figure 6.4: The results for the stream function from the numerical solution. The color contours represent the magnitude of the stream function and are scaled from -6 to 6 for ease of comparison. The arrows show the direction of the flow.

Figure 6.4 above shows the results for the stream function from the numerical solution. For Rayleigh numbers $Ra \geq 80$, three convection cells result.

Analysis and Discussion

Overview

The results from the Lorenz system and the numerical solution are now compared. First, the percent difference is calculated using the following formula,

$$Percent\ Difference = \left|\frac{T_N - T_L}{T_N}\right| \cdot 100\% \tag{6.1}$$

The results for all simulations ($40 \leq Ra \leq 100$) are presented in Figure 6.5 and Figure 6.6. The percent difference shows to what degree the Lorenz system varies from the numerical results as a percent of the value of the numerical. The scale is such that when the Lorenz system is within 5% of the numerical the resulting contour is green. When the Lorenz system varies to a degree greater then 5% of the numerical the result is red.

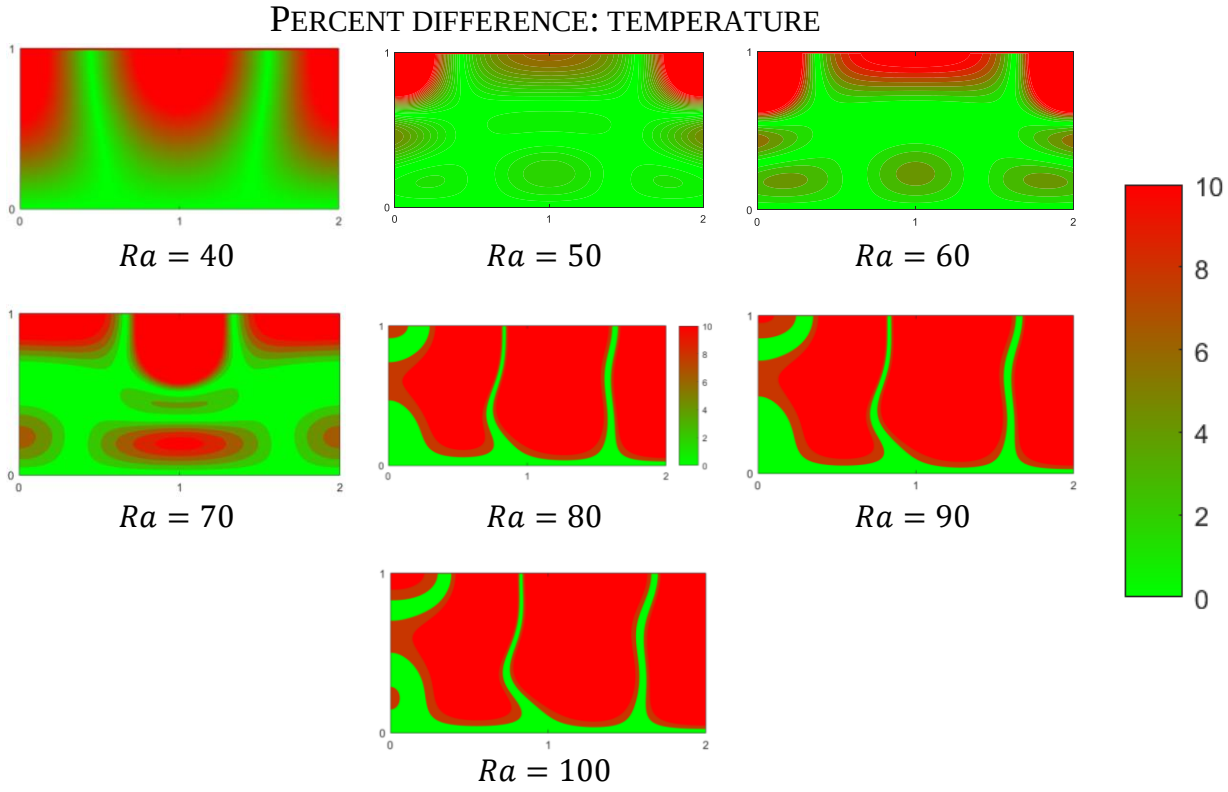

Figure 6.5: The percent difference between the Lorenz system for temperature and the numerical solution for temperature for the range $40 \leq Ra \leq 100$. The Lorenz system shows the greatest degree of agreement with the numerical near $Ra = 50$.

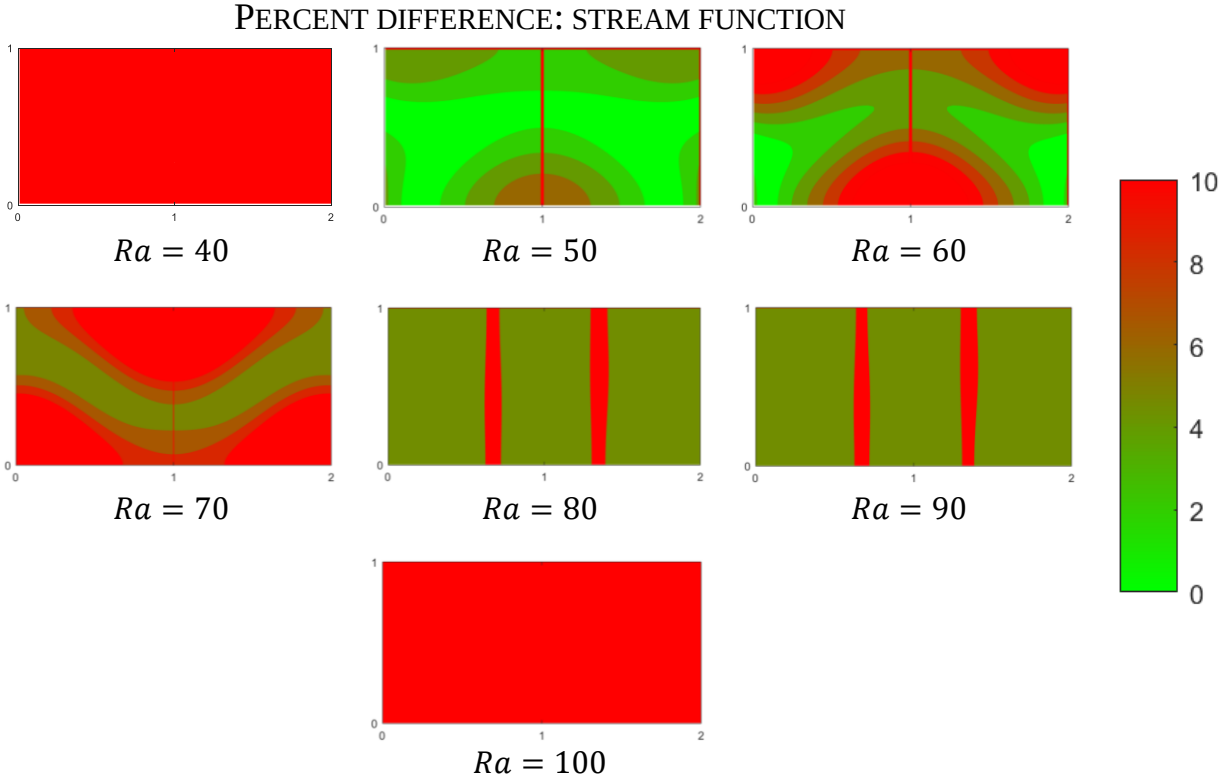

Figure 6.6: The percent difference between the Lorenz system for the stream function and the numerical solution for the stream function for the range $40 \leq Ra \leq 100$. The Lorenz system shows the greatest degree of agreement with the numerical near $Ra = 50$.

The results are now compared by calculating the absolute difference. This value represents the discrepancy between the Lorenz system and the numerical solutions in a way that is not scaled by the value of the numerical solution.

$$Absolute\ Difference = |T_N - T_L| \tag{6.2}$$

The contours for the absolute temperature difference are scaled from 0 to 0.1 on each graph, since the maximum temperature deviation that occurs is ≈ 0.1. The contours for the absolute difference in stream function are scaled from 0 to 0.7 for the same reason.

The results for $Ra = 40$ show an unexpectedly high difference. As a result, this case is addressed in its own section. The results for $Ra = 50$ show the lowest deviation over the problem domain and thus have their own section. The results for Rayleigh numbers $60 \leq Ra \leq 90$ show a consistent increase in deviation and are presented together, so that the evolution of increasing difference can be easily seen. For the case $Ra = 80$, the numerical solution no longer predicts that two convection cells will occur. As a result, this case is addressed separately and the absolute difference is not calculated, as the fundamental nature of the solutions does not agree.

Results for $Ra = 40$

The results from the Lorenz system and numerical solutions show greater than 10% difference in many areas of the problem domain for both temperature and the stream function. Close to the Rayleigh critical number ($Ra_{cr} = 4\pi^2 \approx 39.48$), the convection is very weak, resulting in filtration velocities close to zero. Similarly, close to $z = 1$ the temperature approaches zero. This means that the calculation of percent difference requires dividing by a number close to zero. An alternative analysis is presented which is not scaled by the numerical solution.

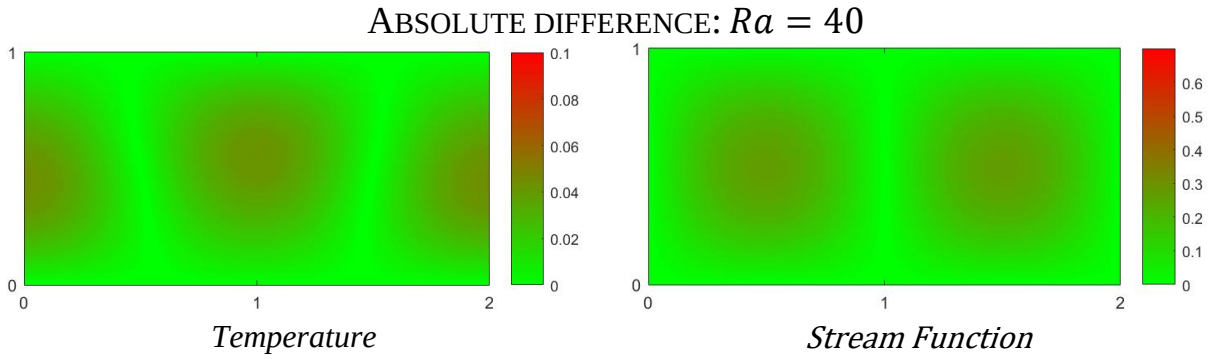

Figure 6.7: The absolute differences for the temperature and stream function for $Ra = 40$.

The absolute difference between the Lorenz system and the numerical solution for $Ra = 40$ is presented above in Figure 6.7. The greatest discrepancy for the stream function occurs at the

center of each of the convection cells. The amplitude of the stream function at the center of the cells is predicted by the Lorenz system to be nearly twice that of the numerical solution, as shown in Table 6-1 below.

Table 6-1: The maximum values for temperature are the same for all Rayleigh numbers, regardless of solution method because the maximum is defined by the boundary conditions of the problem. The maximum value for the stream function is dependent on the Rayleigh number and is often different for the two solution methods. The table below compares the maximum values for the stream function which result from the numerical solution and Lorenz system for $Ra = 40$.

Maximum temperature	$\max(T_N) = 1$
Maximum difference between Lorenz system and numerical temperature solutions	$\max(\lvert T_N - T_L \rvert) = 0.045$
Maximum stream function (Numerical)	$\max(\Psi_N) = 0.21$
Maximum stream function (Lorenz)	$\max(\Psi_L) = 0.48$
Maximum difference between Lorenz system and numerical stream function solutions	$\max(\lvert \Psi_N - \Psi_L \rvert) = 0.27$

These results indicate that the Lorenz system and the numerical solution have significantly different results near the transition point from the motionless solution to the convective solution.

Results for $40 < Ra < 60$

Inspection of Figure 6.5 and Figure 6.6 indicate that the Lorenz system matches the numerical solution to greatest degree in the range of $40 < Ra < 60$. To determine the true validity domain of the Lorenz equations as a model for natural convection in porous media, it is necessary to look in greater detail at the behavior of both the Lorenz system to the numerical solution for this range. Additional trials were ran for the numerical and Lorenz system to determine the Rayleigh number which gives the minimum difference between the two solution methods.

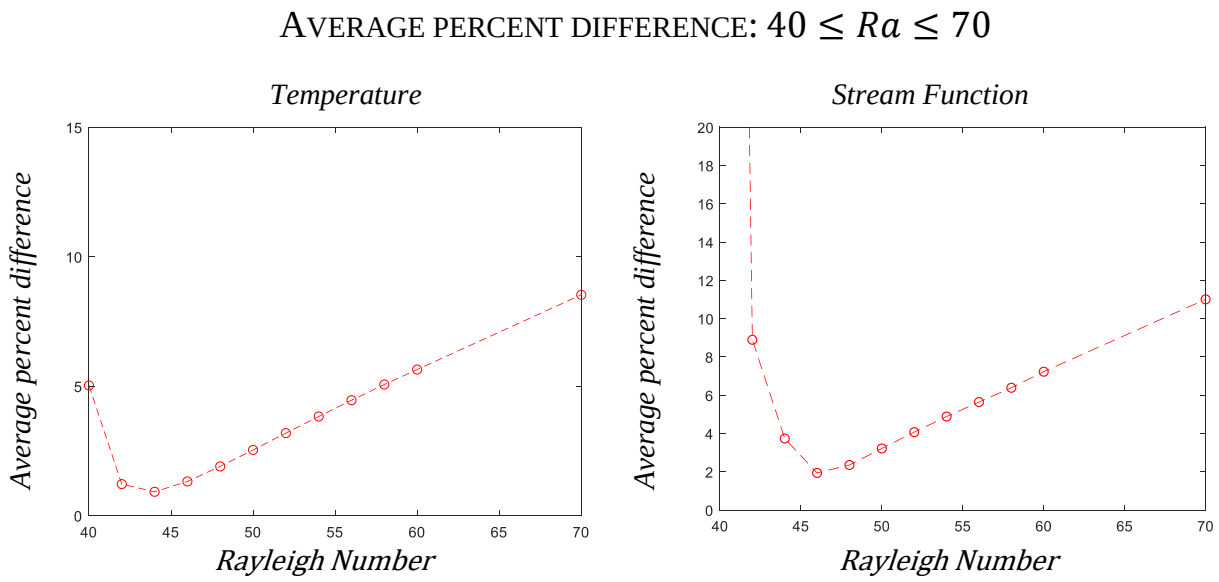

Figure 6.8: The average percent difference between the Lorenz system and the numerical solution, averaged over the whole problem domain.

Inspection of Figure 6.7 and Figure 6.8 indicates that the Lorenz system shows the smallest discrepancy near $Ra = 46$. After this point, the average difference between the two solutions increases linearly. For the range $44 \leq Ra \leq 54$ the Lorenz system shows less than a 5% average deviation from the numerical solution. The absolute difference between the numerical solution and the Lorenz system is shown in Figure 6.9. The absolute difference, averaged over the entire problem domain, is presented in Figure 6.10, and the maximum difference is presented in Table 6-2.

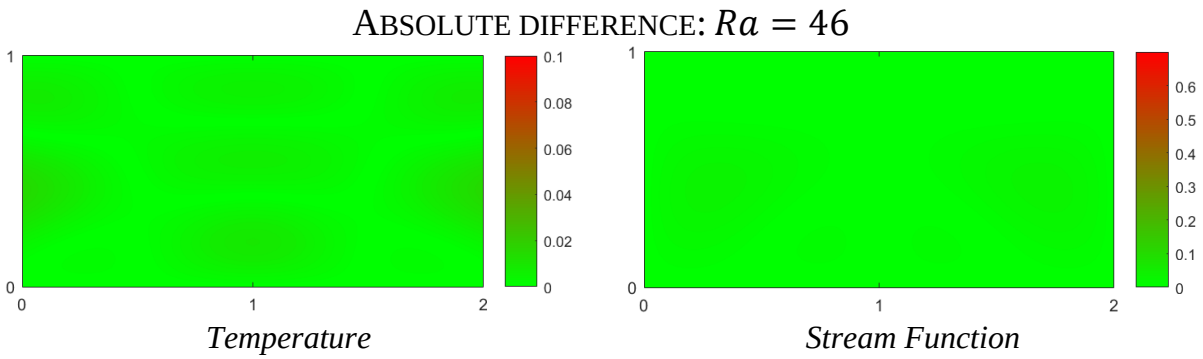

Figure 6.9: The absolute differences for the temperature and stream function for $Ra = 46$.

Table 6-2: The table below shows the maximum absolute difference between the Lorenz system and numerical solution for Rayleigh numbers in the range $40 \leq Ra \leq 60$.

	$\max(T)$	$\max(\lvert T_N - T_L \rvert)$	$\max(\Psi_N)$	$\max(\Psi_L)$	$\max(\lvert \Psi_N - \Psi_L \rvert)$
$Ra = 40$	1	0.045	0.21	0.48	0.27
$Ra = 42$	1	0.018	0.93	1.01	0.081
$Ra = 44$	1	0.016	1.31	1.35	0.05
$Ra = 46$	1	0.015	1.60	1.63	0.03
$Ra = 48$	1	0.015	1.85	1.86	0.027
$Ra = 50$	1	0.019	2.08	2.06	0.049
$Ra = 52$	1	0.024	2.28	2.25	0.071
$Ra = 54$	1	0.029	2.47	2.42	0.095
$Ra = 46$	1	0.034	2.65	2.59	0.119
$Ra = 48$	1	0.039	2.82	2.74	0.146
$Ra = 60$	1	0.043	2.98	2.88	1.175

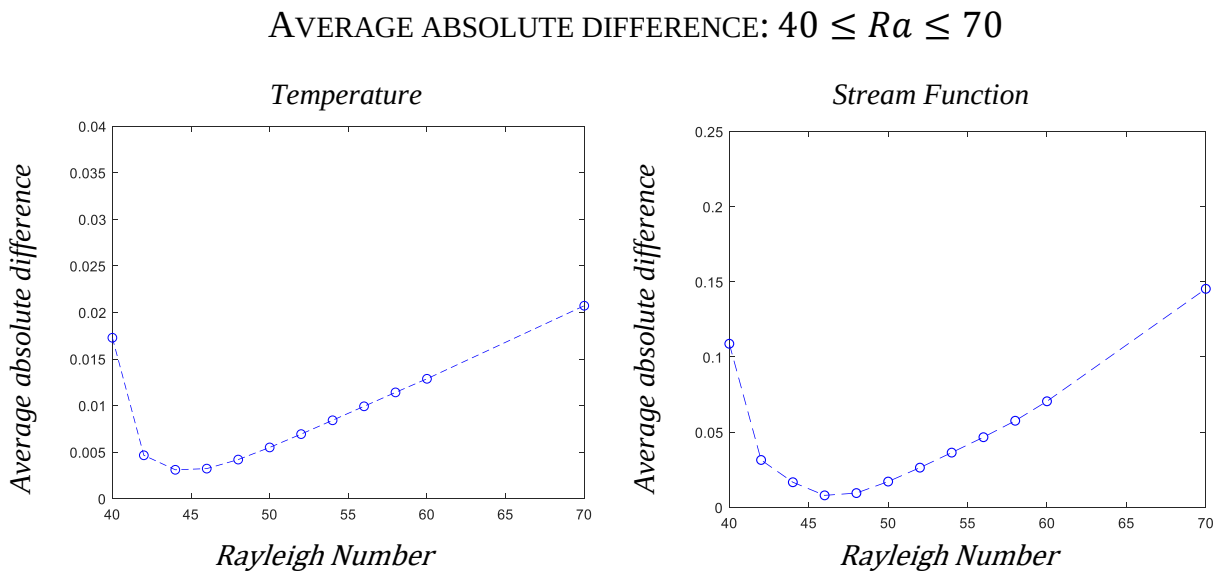

Figure 6.10: The average absolute difference between the Lorenz system and the numerical solution, averaged over the whole problem domain.

This transition period is predicted to occur exactly at the point $Ra = 4 \cdot \pi^2$. This is the point at which, mathematically, the equations predict that the motionless solution will become unstable. However, theoretically, the motionless solution will persist indefinitely if there is no disturbance, as convection cannot be initiated if $\frac{dT}{dx} = 0$. Additionally, experimental results indicate that the transition point can occur slightly before or after this point, depending on the conditions of the experiment. Theoretical understanding of the transition from the motionless solution to the convective solution is still incomplete.

These results indicate that the Lorenz system is best able to predict the results of the numerical solution in the neighborhood of $Ra = 46$. This is presumably the point at which the nature of the solution has transitioned fully from pure conduction to convection.

Results for $60 \leq Ra \leq 70$

The range at which the Lorenz system is able to predict the numerical solution within 5% deviation is $44 \leq Ra \leq 54$. However, up to $Ra = 70$ the Lorenz system and numerical solutions both predict that two convection cells will result. The absolute differences for the temperature and stream function are presented below in Figure 6.11 and Figure 6.12, and the maximum difference that occurs in the problem domain between the Lorenz system and the numerical solution is presented in Table 6-3.

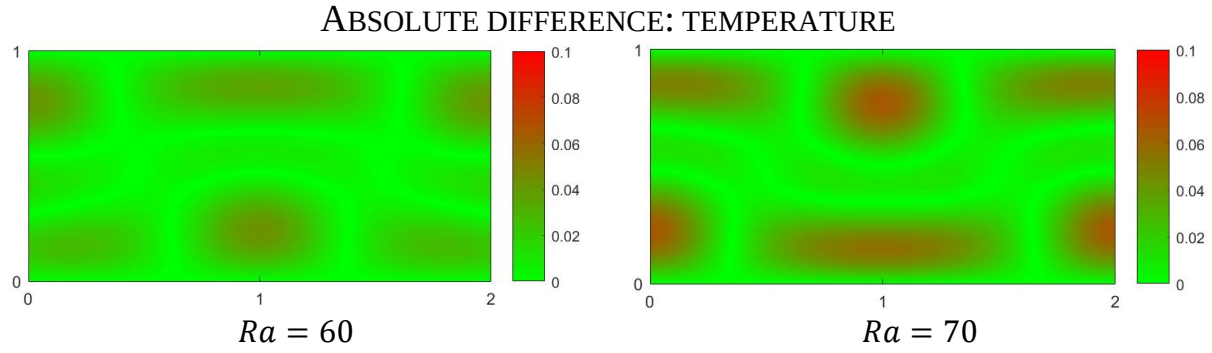

Figure 6.11: The absolute difference between the Lorenz system and numerical temperature solutions for $60 \leq Ra \leq 70$.

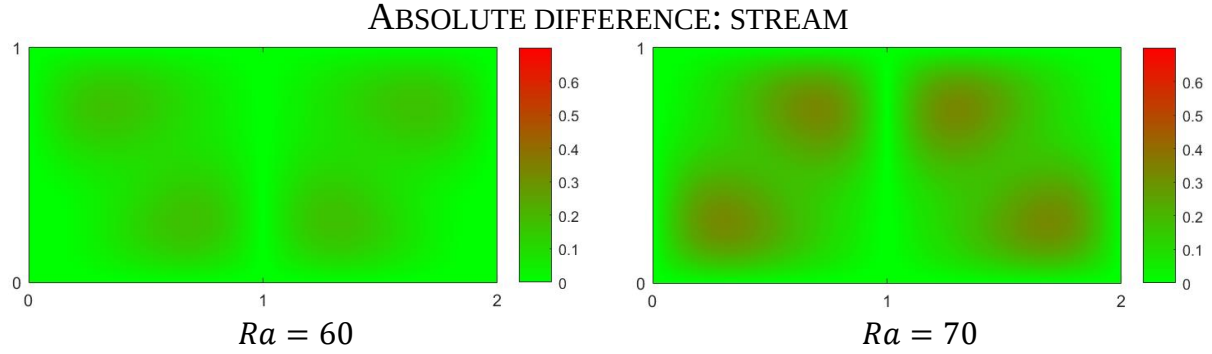

Figure 6.12: The absolute difference between the Lorenz system and numerical stream function solutions for $60 \leq Ra \leq 70$.

Table 6-3: The table below compares the maximum values for the stream function which result from the numerical and Lorenz system for $60 \leq Ra \leq 70$

	$\max(T)$	$\max(\lvert T_N - T_L \rvert)$	$\max(\Psi_N)$	$\max(\Psi_L)$	$\max(\lvert \Psi_N - \Psi_L \rvert)$
$Ra = 60$	1	0.043	2.98	2.88	0.175
$Ra = 70$	1	0.066	3.71	3.52	0.330

Results for $Ra \geq 80$

When the Rayleigh number reaches $Ra = 80$, the numerical solution no longer predicts that two convection cells will occur. The formation of two convection cells is one of the fundamental assumptions for the Lorenz system. As a result, the Lorenz system and numerical solutions fundamentally disagree on the nature of the solution that will result. It has been shown experimentally that the size of the convection cells that form decreases slightly in length as the Rayleigh number increases. This phenomenon was discussed in Chapter 2

Comparison of analytical results with experimental data

The results from both the Lorenz system and numerical simulations are now compared with experimental data. When natural convection is studied experimentally, the quantity measured is the average Nusselt number. The average Nusselt number was calculated using the results from the simulation. Chapter 4 outlines the process for analyzing the raw experimental data. Figure 6.13 shows the relationship between the Nusselt number and the Rayleigh number for the experimental data compared to the results from the Lorenz system and numerical solutions.

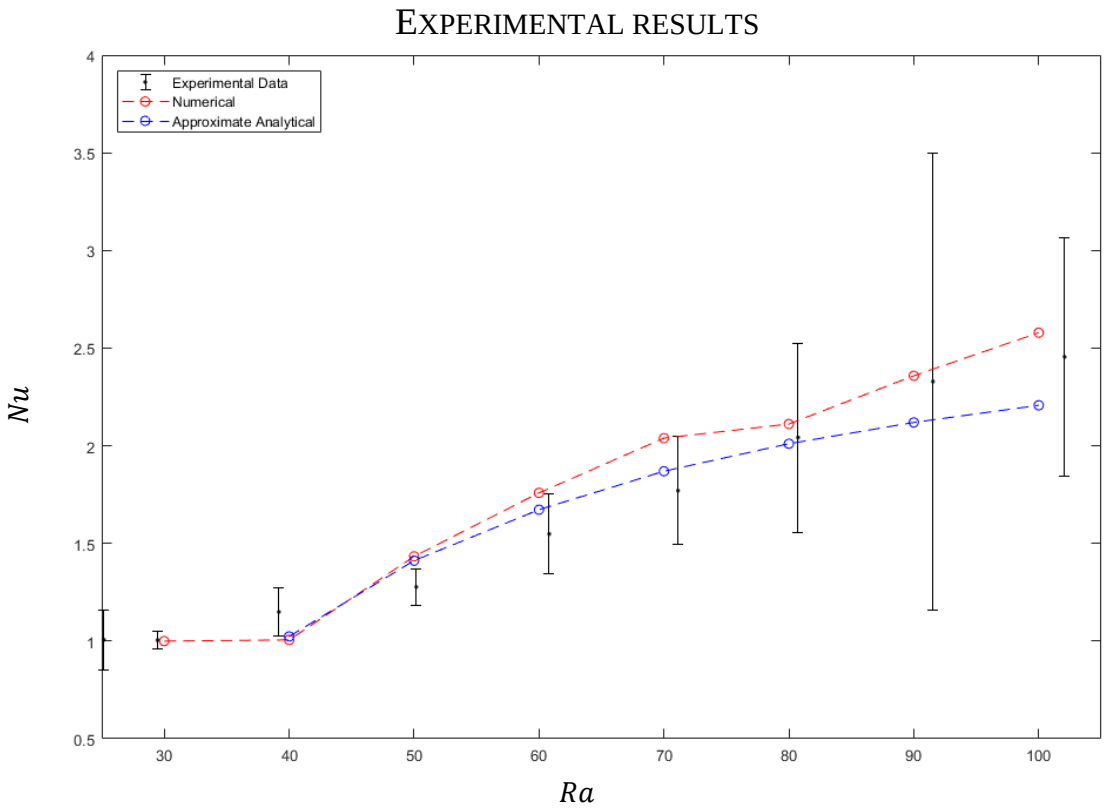

Figure 6.13: The experimental data for Nusselt vs. Ralyeigh number with the computational results for the Nusselt number from the Lorenz system and numerical solutions. The error bars represent a 95% confidence interval.

Figure 6.13 shows that both the Lorenz system and numerical models are inadequate for predicting the Nusselt number when the Rayleigh number is close to the critical Rayleigh number. However, the Lorenz system results (shown in blue) fall within the 95% confidence interval for the range $60 \leq Ra \leq 100$, while the numerical results (shown in red) fall within the experimental error bars for the range $75 \leq Ra \leq 100$.

It is possible that imperfect experimental conditions such as uneven heating of bottom or imperfectly insulated side walls may have caused an imperfect bifurcation to occur, as discussed in Chapter 3 resulting in greater than predicted Nusselt numbers close to the transition point. No information regarding the tolerances to which the experimental boundary conditions were held

was present in the publications, so it cannot be known to what extent these imperfections may have affected the experimental results.

7 CONCLUSIONS

The purpose of this research was to determine the validity domain of the Lorenz equations as a model for natural convection in porous media, i.e. for which Rayleigh numbers are the Lorenz equations valid as a model for natural convection. One would assume that a straightforward question such as this would result in a straightforward answer. However, the nature of this universe dictates that even the most straightforward questions have complex answers. The work presented here represents a mere first step into understanding the merits and drawbacks of this model, and no number of plots and tables can do sufficient justice to the complex mathematical beauty of the problem of natural convection in porous media. With that concession, the practical uses and limitations of the Lorenz system are henceforth presented, within the bounds of $40 \leq Ra \leq 100$.

Conclusions for range $Ra = 40$

Near the critical Rayleigh number the Lorenz system accurately predicts neither the temperature contours nor the stream function to sufficient accuracy. Additionally, when compared with experimental data, the Lorenz system under predicts the Nusselt number.

Conclusions for range $40 < Ra < 60$

The range for which the Lorenz system is able to predict the numerical solution within 5% is $44 \leq Ra \leq 54$. The Lorenz system shows the best prediction at $Ra = 46$. However, for this range of Rayleigh numbers neither the Lorenz system nor the numerical solutions fall within the 95% confidence interval.

Conclusions for range $60 \leq Ra \leq 70$

For this range of Rayleigh number, the percent difference and absolute difference both increase in an approximately linear fashion. The Lorenz system does not agree with the numerical solution within 5%, on average. However, the Lorenz system falls within the experimental 95% confidence interval for this range.

Conclusions for range $Ra \geq 80$

The fundamental nature of the solution changes at $Ra = 100$. The Lorenz system makes the assumption that two convection cells will result. However, the results for the numerical solution suggest that after $Ra = 100$, three or more convection cells may form. The experimental data indicates that both the Lorenz system and numerical solutions can predict the Nusselt number for this range, though the Lorenz system is closer to the mean than the numerical for $Ra = 100$. To correctly predict the behavior of the solution for Rayleigh numbers greater than $Ra = 100$, it will be necessary to study experimentally and theoretically the effect of the Rayleigh number on the number of convection cells that form. More experimental data is also needed to make a comparison of the Nusselt number.

REFERENCES

[1] M. Quintard *et al.*, *Handbook of Porous Media*, 3rd ed. Boka Raton, FL: Taylor & Francis Group, 2015.

[2] P. Cheng, "Heat Transfer in Geothermal Systems," *Adv. Heat Transf.*, vol. 14, no. October, pp. 1–105, 1978.

[3] H. Darcy, "Les fontaines publiques de la ville de Dijon," *Recherche*, p. 647, 1856.

[4] P. Vadasz and S. Olek, "Computational recovery of the homoclinic orbit in porous media convection," *Int. J. Non. Linear. Mech.*, vol. 34, no. 6, pp. 1071–1075, 1999.

[5] E. N. Lorenz, "Deterministic Nonperiodic Flow," *J. Atmos. Sci.*, vol. 20, no. 2, pp. 130–141, 1963.

[6] T. Kaneko, M. F. Mohtadi, and K. Aziz, "An experimental study of natural convection in inclined porous media," *Int. J. Heat Mass Transf.*, vol. 17, pp. 485–496, 1974.

[7] P. Vadasz, "Heat flux dispersion in natural convection in porous media," *Int. J. Heat Mass Transf.*, vol. 53, no. 17–18, pp. 3394–3404, 2010.

[8] M. A. Combarnous and S. A. Borries, "Hydrothermal convection in saturated porous media," *Adv Hydrosci*, vol. 10, pp. 231–307, 1975.

[9] P. Vadasz and S. Olek, "Transitions and chaos for free convection in a rotating porous layer," *Int. J. Heat Mass Transf.*, vol. 41, no. 11, pp. 1417–1435, 1998.

[10] P. Vadasz, "Local and Global Transitions to Chaos and Hysteresis in a Porous Layer Heated from Below," *Transp. Porous Media*, vol. 37, pp. 213–245, 1999.

[11] S. Chandrasekhar, *Hydrodynamic and Hydromagnetic Stability*. 1962.

[12] J. M. Straus, "Large amplitude convection in porous media," *J. Fluid Mech.*, vol. 64, no. 1, pp. 51–63, 1974.

[13] P. Vadasz, 2018, Professor at Northern Arizona University, private communication.

[14] P. Vadasz, "Subcritical transitions to chaos and hysteresis in a fluid layer heated from below," *Int. J. Heat Mass Transf.*, vol. 43, no. 5, pp. 705–724, 2000.

[15] P. Vadasz and S. Olek, "Route to chaos for moderate Prandtl number convection in a porous layer heated from below," *Transp. Porous Media*, vol. 41, no. 2, pp. 211–239, 2000.

[16] P. Vadasz, "Controlling chaos in porous media convection by using feedback control," *Transp. Porous Media*, vol. 85, no. 1, pp. 287–298, 2010.

[17] P. Vadasz, "Equivalent initial conditions for compatibility between analytical and computational solutions of convection in porous media," *Int. J. Non. Linear. Mech.*, vol. 36, no. 2, pp. 197–208, 2001.

[18] P. Vadasz and S. Olek, "Weak turbulence and chaos for low Prandtl number gravity driven convection in porous media," *Transp. Porous Media*, vol. 37, no. 1, pp. 69–91, 1999.

[19] P. Vadasz, "Analytical prediction of the transition to chaos in Lorenz equations," *Appl. Math. Lett.*, vol. 23, no. 5, pp. 503–507, 2010.

[20] P. Vadasz, "Capturing analytically the transition to weak turbulence and its control in porous media convection," *J. Porous Media*, vol. 118, no. 11, pp. 1075–1089, 2015.

[21] B. Tummers, “Data Thief III,” *Http://Datathief.Org/*, 2006. [Online]. Available: http://datathief.org/. [Accessed: 15-Dec-2017].

[22] P. Vadasz and C. Braester, “The effect of imperfectly insulated sidewalls on natural convection in porous media,” *Acta Mech.*, vol. 91, no. 3–4, pp. 215–233, 1992.

[23] P. J. Roache, “Code Verification by the Method of Manufactured Solutions,” *J. Fluids Eng.*, vol. 124, no. 1, p. 4, 2002.

[24] “Standard for Verification and Validation in Computational Fluid Dynamics and Heat Transfer.” 2009.

APPENDIX

Appendix I: Numerical solver

MATLAB Function: RUN.m

```
function [Stream_N,Temp_N] = RUN(Ra,N,Va)

    if ~exist('Ra','var')
        %Default Rayleigh number
        Ra = 45;
    end
    if ~exist('N','var')
        %Default grid spacing
        N = 60;
    end

    if ~exist('Va','var')
        %Default Vadasz number
        Va = 98.7;
    end

    foldername = sprintf('RA%d_N%d',Ra,N);

    mkdir(foldername)

    %Time step
    if Ra < 500
        deltaT = 2/N/2;
    else
        deltaT = 2/N/20;
    end

    %Length in x-direction (Aspect Ratio)
    L = 3;

    %Space between gridpoints in x-direction
    deltaL = L/N;

    %Gridpoints in y-direction
    M = (1/deltaL)+1;

    %Gridpoints in x-direction
    N = N+1;

    %%% Initialize Temperature Mesh %%%
    Temperature = zeros(M*N,1);

    for i = 1:N
        Temperature(i) = 1;
    end
```

```
    for i = [randi([N+1,(M-1)*N]),randi([N+1,(M-1)*N])]
        Temperature(i) = 1;
    end

    %%% Initialize Stream Mesh %%%
    %Zero velocity in x and y direction everywhere
    Stream = zeros(M*N,1);

    %%% Initialize necessary variables %%%
    global constants_g
    global initial_stream_g
    global initial_temp_g

    global stop

    constants_g = [M;N;deltaL;deltaT;Ra;Va];
    initial_stream_g = Stream;
    initial_temp_g = Temperature;

    stop = false;

    %%% Pass initial conditions and necessary parameters to solver %%%
    [Stream_N,Temp_N] = Controller;

    Stream_N = vec2mat(Stream_N,N);
    Temp_N = vec2mat(Temp_N,N);

End
```

MATLAB Function: Iterate.m

```
function [Stream_jp1,Temp_jp1] = Iterate(Stream_j,Temp_j)

format long

global stop

global constants_g

constants = constants_g;

Va = constants(6);
Ra = constants(5);
deltaT = constants(4);
deltaL = constants(3);
N = constants(2);
M = constants(1);

S_done = false;
T_done = false;

Temp_jp1a = Temperature(Stream_j,Temp_j);
Stream_jp1a = StreamFunction(Stream_j,Temp_jp1a);

foldername = sprintf('RA%d_N%d',Ra,N-1);

i=1;
s_diff = [];
t_diff = [];
tic
while ((S_done == false)||(T_done == false)) && stop == false

    Temp_jp1b = Temperature(Stream_jp1a,Temp_j);
    Stream_jp1b = StreamFunction(Stream_j,Temp_jp1b);
    S_diff = sum(abs(Stream_jp1b - Stream_jp1a));
    T_diff = sum(abs(Temp_jp1b - Temp_jp1a));

    if S_diff < .00000001
        S_done = true;
    end

    if T_diff < .00000001
        T_done = true;
    end

    s_diff(i) = S_diff;
    t_diff(i) = T_diff;

    Stream_jp1a = Stream_jp1b;
    Temp_jp1a = Temp_jp1b;

    i = i+1;
end
elapsedtime = toc;
```

```
cd(foldername)
dlmwrite('timeElapsed.txt',elapsedtime,'-append');
cd ..

%%% Outputs
Stream_jp1 = Stream_jp1a;
Temp_jp1 = Temp_jp1a;
```

MATLAB Function: Controller.m

```
function [Stream_N, Temp_N] = Controller()

format long

global constants_g;
global initial_stream_g;
global initial_temp_g;

global stop

Temp_j = initial_temp_g;
Stream_j = initial_stream_g;

constants = constants_g;

Va = constants(6);
Ra = constants(5);
deltaT = constants(4);
deltaL = constants(3);
N = constants(2);
M = constants(1);

foldername = sprintf('RA%d_N%d',Ra,N-1);

%Max number of time steps solver will take
p = 10000000;

%Initialize conditions that allow solver to check for steady state
S_done = false;
T_done = false;

%Very first step forward in time
Temp_jp1a = Temperature(Stream_j,Temp_j);
Stream_jp1a = StreamFunction(Stream_j,Temp_jp1a);

j=2;

%Times how long each step forward in time takes to compute
tic

%While loop continues to move the solution forward in time as long as the
%temperature and stream functions are both changing, or when the max number
%of time steps has been reached.
while ((S_done == false)||(T_done == false)) && (j<p) && stop == false

    [Stream_jp1,Temp_jp1] = Iterate(Stream_j,Temp_j);

%     Temp_field(:,j) = Temp_jp1;
%     Stream_field(:,j) = Stream_jp1;

    S_diff = sum(abs(Stream_jp1 - Stream_j));
    T_diff = sum(abs(Temp_jp1 - Temp_j));

    Stream_j = Stream_jp1;
```

```
    Temp_j = Temp_jp1;

    %Check for Stream steady state
    if S_diff < 0.000001
        S_done = true;
    end

    %Check for Temperature steady state
    if T_diff < 0.000001
        T_done = true;
    end

    %Computed temp and stream fields become the new initial conditions for
    %the next time step
    Stream_j = Stream_jp1;
    Temp_j = Temp_jp1;

    cd(foldername)

    dlmwrite('Residual2S.txt',full(S_diff),'-append');
    dlmwrite('Residual2T.txt',full(T_diff),'-append');

    dlmwrite('Stream.txt',full(Stream_j));
    dlmwrite('Temp.txt',full(Temp_j));

    cd ..

    j = j+1;
end

elapsedtime = toc;

%%% Outputs %%%
Stream_N = Stream_j;
Temp_N = Temp_j;
```

MATLAB Function: StreamFunction.m

```
function [Stream_jp1] = StreamFunction(Stream_j,Temp_jp1)

format long

global constants_g
constants = constants_g;

Va = constants(6);
Ra = constants(5);
deltaT = constants(4);
deltaL = constants(3);
N = constants(2);
M = constants(1);

%%% Knowns %%%
temp_jp1 = Temp_jp1;
stream_j = Stream_j;

a = Va*deltaT+1;
b = 1;
c = -0.5*Ra*Va*deltaT*deltaL;

%Preallocate space for B
B = sparse(M*N,1);

for i = 1:M*N
    if (0 < i)&&(i <= N)
        B(i) = 0;
    elseif mod(i,N) == 1
        B(i) = 0;
    elseif mod(i,N) == 0
        B(i) = 0;
    elseif (N*(M-1) < i)&&(i <= M*N)
        B(i) = 0;
    else
        B(i) = (c*(temp_jp1(i+1)-temp_jp1(i-1))) + b*(stream_j(i+1) +
stream_j(i+N) - 4*stream_j(i) + stream_j(i-N) + stream_j(i-1));
    end
end

%%% Unknowns %%%

b = zeros(M*N,5);

%a_imN
b(:,1) = a;
b(1:N:(M-1)*N+1,1) = 0;
b(N:N:(M-1)*N,1) = 0;
b((M-2)*N:(M-1)*N,1) = 0;

%a_im1
b(:,2) = a;
b(1:N,2) = 0;
b(N-1:N:(M-1)*N-1,2) = 0;
```

```
b(N:N:(M-1)*N,2) = 0;
b((M-1)*N:M*N,2) = 0;

%a_i
b(:,3) = -4*a;
b(1:N,3) = 1;
b(N+1:N:(M-1)*N+1,3) = 1;
b(N:N:(M-1)*N,3) = 1;
b((M-1)*N:M*N,3) = 1;

%a_ip1
b(:,4) = a;
b(1+1:N+1,4) = 0;
b(N+1+1:N:(M-1)*N+1+1,4) = 0;
b(N+1:N:(M-1)*N+1,4) = 0;
b((M-1)*N+1:M*N+1,4) = 0;

%a_ipN
b(:,5) = a;
b(1+N:N+N,5) = 0;
b(N+1+N:N:(M-1)*N+1+N,5) = 0;
b(N+N:N:(M-1)*N+N,5) = 0;

d = [-N,-1,0,1,N];

A = spdiags(b,d,M*N,M*N);

Solution = A\B;

%%% Outputs %%%
Stream_jp1 = Solution;
```

MATLAB Function: Temperature.m

```
function [Temp_jp1] = Temperature(Stream_jp1,Temp_j)

format long

global constants_g
constants = constants_g;

N = constants(2);
M = constants(1);
Va = constants(6);
Ra = constants(5);
deltaT = constants(4);
deltaL = constants(3);

%%% Knowns %%%
B = sparse(Temp_j);
% Stream = vec2mat(Stream_jp1,N);
Stream = Stream_jp1;

%Take stream function from previous time step and extract x and z direction
%velocities
u_j = zeros(M*N,1);
w_j = zeros(M*N,1);

for i = 1:M*N
    if mod(i,N) == 1
        w_j(i) = 0;
        u_j(i) = 0;
    elseif mod(i,N) == 0
        w_j(i) = 0;
        u_j(i) = 0;
    elseif (i <= N)
        w_j(i) = 0;
        u_j(i) = 0;
    elseif (N*(M-1) < i)
        w_j(i) = 0;
        u_j(i) = 0;
    else
        u_j(i) = (Stream(i-1) - Stream(i+1))/(2*deltaL);
        w_j(i) = (Stream(i+N) - Stream(i-N))/(2*deltaL);
    end
end

% [u_j,w_j] = gradient(Stream);
%
% u_j = reshape(u_j./(-deltaL),[1,M*N]);
% w_j = reshape(w_j./(deltaL),[1,M*N]);

%Problem Constants
s = deltaT/(2*deltaL);
r = deltaT/deltaL^2;

%Matrix Coefficients
a_imN = -(s.*u_j+r);
```

```
a_im1 = -(s.*w_j+r);
a_i   =  (4*r+1.*ones(M*N,1));
a_ip1 = -(-s.*w_j+r);
a_ipN = -(-s.*u_j+r);

%%% Unknowns %%%

b = zeros(M*N,5);
b(:,1) = a_imN;
b(1:N:(M-2)*N+1,1) = -r;
b(N:N:(M-2)*N,1) = -r;
b((M-2)*N+1:(M-1)*N+1,1) = 0;

b(:,2) = a_im1;
b(1:N-1,2) = 0;
b(N:N:(M-1)*N,2) = 0;
b((M-1)*N:M*N,2) = 0;
b(2*N-1:N:(M-1)*N-1,2) = -2*r;

b(:,3) = a_i;
b(1:N,3) = 1;
b((M-1)*N+1:M*N,3) = 1;

b(:,4) = a_ip1;
b(1+1:N+1,4) = 0;
b(N+1+1:N:(M-2)*N+1+1,4) = -2*r;
b(2*N+1:N:(M-1)*N+1,4) = 0;
b((M-1)*N+1:M*N,4) = 0;

b(:,5) = a_ipN;
b(1+N:N+N,5) = 0;
b(N+1+N:N:(M-1)*N+1+N,5) = -r;
b(2*N+N:N:(M-1)*N+N,5) = -r;


d = [-N,-1,0,1,N];

A = spdiags(b,d,M*N,M*N);

A_t = A;
B_t = B;

Solution = A\B;
%[Solution,~] = bicgstabl(A,B,1e-10,500);

%%% Outputs %%%
Temp_jp1 = Solution;
```

Appendis II: Lorenz solver

```
function [Stream_A,Temp_A] = RUN_A(Ra,N,Va)

if ~exist('Ra','var')
    %Default Rayleigh number
    Ra = 45;
end
if ~exist('N','var')
    %Default grid spacing
    N =60;
end

if ~exist('Va','var')
    %Default Vadasz number
    Va = 98.7;
end
if ~exist('x0','var')
    x0 = 111;
end
if ~exist('y0','var')
    y0 = 15;
end
if ~exist('z0','var')
    z0 = 1;
end

R = Ra/(4*pi^2);
M = N/2;

foldername = 'Z:\Documents\Thesis Data\';
foldername =
horzcat(foldername,sprintf('Ra%d',Ra),'\',sprintf('RA%d_N%d',Ra,N));
workingdirectory = pwd;

alpha = Va/(2*pi^2);
g=@(t,x)[alpha*(x(2)-x(1));-x(2)+R*x(1)-(R-1)*x(1)*x(3);2*(x(1)*x(2)-x(3))];

Y0 = [x0,y0,z0];

[t,xa] = ode23(@(t,x) g(t,x),[0,100],Y0);

A_11 = (-4*(R-1)^0.5).*xa(:,1);
B_11 = (2*(R-1)^0.5)/(pi*R).*xa(:,2);
B_02 = -(R-1)/(pi*R).*xa(:,3);

x_vec = pi*linspace(0,2,N+1);
z_vec = pi*linspace(0,1,M+1);

sin_x = sin(x_vec);
sin_z = sin(z_vec);
cos_x = cos(x_vec);
sin_2z = sin(2.*z_vec);

for i = 1:length(sin_x)
```

```
    sin_xsin_z(i,:) = sin_x(1,i).*sin_z';
end

for i = 1:length(sin_x)
    a(i,:) = cos_x(1,i).*sin_z';
    b(i,:) = sin_2z';
    c(i,:) = 1-(z_vec./pi)';
end

for i = 1:length(t)
    Stream_field(:,:,i) = A_11(i).*sin_xsin_z;
    Temp_field(:,:,i) = B_11(i).*a + B_02(i).*b + c;
end

Stream_A = Stream_field(:,:,length(t))';
Temp_A = Temp_field(:,:,length(t))';

cd(foldername)

dlmwrite('StreamA.txt',Stream_A);
dlmwrite('TempA.txt',Temp_A);

cd(workingdirectory)

end
```